**Joule** 



#### **Review**

# Energetic and dynamic principles of potassium electrodeposition in potassium metal batteries

Yupei Han (韩玉培),1,2 Pan He (何攀),1,2 and Yang Xu (徐杨)1,\*

<sup>1</sup>Department of Chemistry, University College London, London WC1H 0AJ, UK

https://doi.org/10.1016/j.joule.2025.102053

CONTEXT & SCALE The pursuit of high-energy, low-cost, and sustainable energy storage has renewed interest in potassium metal batteries (PMBs) that offer natural abundance, low material cost, and favorable electrochemical properties. However, uncontrolled potassium (K) dendrite growth remains a critical barrier to the practical deployment of PMBs. Although studies have investigated materials and interfacial engineering strategies to mitigate K dendrite formation, the fundamental mechanisms that govern K nucleation and early-stage growth, which ultimately drive dendrite development, are still not fully understood.

This review addresses this knowledge gap by establishing a theoretical framework to describe K electrode-position from both thermodynamic and kinetic perspectives. Key interfacial parameters, including contact angle, surface energy, interfacial energy, and binding energy, are systematically analyzed to explain nucleation behavior and inform substrate design. The combined effects of binding and interfacial energies are also explored in alloying systems to demonstrate how K nucleation can be selectively promoted and controlled. In parallel, solid-electrolyte interphase (SEI) is examined as a dynamic and functional interface. Its mechanical strength and ionic conductivity are identified as critical factors that influence interfacial stability and deposition morphology. Strategies for enhancing SEI performance through materials and electrolyte engineering are reviewed in detail.

By integrating energetic principles with recent advances in interfacial chemistry and materials design, this review presents a principle-based framework for suppressing dendrite formation and achieving reversible K metal plating. It also outlines future research directions, including *in situ* and *operando* characterization, rational electrolyte formulation, and multiscale modeling, to improve understanding of SEI evolution and electrodeposition dynamics. Overall, this work bridges theoretical understanding and practical strategies, providing guidance for the rational design of stable K metal anodes and accelerating the development of scalable, high-performance PMBs.

#### **SUMMARY**

Potassium metal batteries offer a sustainable and cost-effective solution for high-energy storage applications. However, uncontrolled potassium dendrite growth remains a major obstacle to achieving long-term stability. In this review, we provide a holistic overview by establishing a theoretical framework for potassium nucleation and early-stage growth, identifying key factors that influence stable electrodeposition. We discuss representative materials and substrate design strategies that address these factors and emphasize the importance of several energetic parameters, including contact angle, surface energy, interfacial energy, binding energy, and combined binding/interfacial energies. These descriptors offer insight into the thermodynamic and kinetic processes governing potassium deposition. In addition, we explore the dynamic role of the solid-electrolyte interphase, particularly its mechanical properties and ionic conductivity, which critically impact deposition behavior. Finally, we outline future research directions toward a principle-driven, knowledge-based approach for regulating potassium electrodeposition, aiming to lay the groundwork for the practical development of next-generation potassium metal batteries.



<sup>&</sup>lt;sup>2</sup>These authors contributed equally

<sup>\*</sup>Correspondence: y.xu.1@ucl.ac.uk





#### INTRODUCTION

Alkali metal batteries have come into the research spotlight in the quest for high-energy batteries to combat carbon emissions and achieve the net-zero goal. 1-3 Utilizing alkali metal anodes (Li, Na, or K) can result in an over two-fold gravimetric energy improvement compared with conventional ion-insertion anodes, with the gravimetric capacities of 3,861 (Li), 1,165 (Na), and 678 mAh g<sup>-1</sup> (K) versus 372 mAh  $g^{-1}$  for LiC<sub>6</sub>, 250–350 mAh  $g^{-1}$  for Na in hard carbons and 279 mAh g<sup>-1</sup> for KC<sub>8</sub>. Despite the high gravimetric capacity of Li metal anodes, the scarcity of Li, constituting merely 0.0017 wt.% of the Earth's crust, along with its rapid consumption, uneven global distribution, and supply-chain challenges, is raising concerns about long-term sustainability and feasibility. Emerging Na and K metal anodes are excellent alternatives to Li metal anodes, owing to their abundance (2.36 wt.% for Na and 2.09 wt.% for K) and exemption from geographic and geopolitical restrictions. Compared with Na, K holds the advantages of a lower electrodeposition potential by 0.23 V in propylene carbonate (PC) solvents and a smaller Stokes radius (3.6 Å for K ions versus 4.6 Å for Na ions), which can translate to a higher cell voltage and better rate capability. 4 These favorable attributes establish potassium metal batteries (PMBs) as a promising candidate for next-generation energy storage systems.

K electrodeposition is undoubtedly critical to the successful operation of PMBs. However, it is highly susceptible to uncontrolled K nucleation and growth, leading to high nucleation overpotential and locally amplified K-ion flux. These effects contribute to K dendrite formation, which can penetrate the separator and potentially cause thermal runaway or even fires. While sizeable K-ion insertion in the cathode also presents challenges, ongoing progress in potassium-ion batteries (PIBs) has led to the development and optimization of numerous K cathode materials, many of which can be readily adapted for PMBs. Excellent summaries of K cathodes are available in previous reviews. 5,6 By contrast, K dendrite growth at the K metal anode remains a major unsolved issue. Furthermore, K electrodeposition is intricately influenced by the solid-electrolyte interphase (SEI), whose formation, stability, and dynamic evolution throughout cycling are not yet fully understood. Although recent studies indicate progress toward unraveling these complexities, the interplay between K electrodeposition and SEI appears extremely complex. Achieving long-term stable K metal plating and stripping is essential not only for the practical use of PMBs but also for enabling a near-stoichiometric anode-to-cathode ratio.8 Minimizing excess K metal usage is imperative for enhancing safety and mitigating risks associated with PMB operation.9

Research on stabilizing K electrodeposition has progressed in recent years, with many studies focusing on improving overall K metal anode performance. While various strategies have been proposed, the fundamental mechanisms underlying these approaches are not always well established. As the development of K metal anodes is still in its early stages, the emergence of diverse strategies, even sometimes demonstrating effectiveness unexpectedly, reflects the exploratory nature of the field. To facilitate systematic progress, a holistic perspective on K electrodeposition, combined with a comprehensive understanding of K nucleation and early-stage growth mechanisms, is essential.

Developing these fundamental insights will help integrate seemingly independent studies and establish a structured framework for designing effective strategies, ultimately driving further advancements in PMBs.

This review endeavors to bridge fundamental principles with recent advances in achieving stable K electrodeposition. It outlines key factors derived from theoretical frameworks, progressing from contact angle, surface energy, and interfacial energy to binding energy, then to the combined effects of binding and interfacial energies, and further to the role of the SEI, reflecting the evolving understanding of K electrodeposition. Additionally, it delves into innovative material and substrate design strategies anchored in these key factors, emphasizing established knowledge while identifying open questions to guide future research on K metal anodes. From a comprehensive yet distinctive perspective, this review seeks to catalyze broader discussions on K electrodeposition and its profound implications for the future of PMBs.

## K NUCLEATION AND GROWTH DURING ELECTRODEPOSITION

Nucleation is a critical process to initiate the formation of new crystals, specifically K crystals in this context. During PMB charging, K metal deposition takes place at the anode surface, either metallic K or the current collector, as shown in Figure 1. Under an applied potential, K ions are released from the cathode material, traverse the cathode-electrolyte interphase (CEI), become solvated by the electrolyte molecules, diffuse toward the anode, shed their solvation shell at the interface of the electrolyte and SEI, traverse the SEI, and form K adatoms (adsorbed atoms) at the SEI/anode interface. Before nucleation can occur, the K adatoms adhere to the anode surface, creating an adsorption layer. Once a sufficient number of adatoms converge at a particular location on the anode surface, they coalesce to form a critical cluster or nucleus, which serves as the foundational point for the subsequent growth of K crystals.<sup>10</sup>

For a cluster to stabilize and grow, it must first overcome the nucleation barrier, the energy required for K adatoms to transition from a disordered state to an orderly crystalline structure on the anode surface. This barrier is influenced by factors such as applied voltage, anode surface properties, electrolyte composition, and the presence of impurities or additives. 11 Once the critical cluster stabilizes, growth occurs through the sequential addition of K atoms, which adsorb onto the anode surface, diffuse, and integrate into the growing crystal. The growth mode varies depending on the nucleation scenario and may follow any of the mechanisms in Figure 2B, including the Frank-van der Merwe, Stranski-Krastanov, or Volmer-Weber models.<sup>12</sup> The Frank-van der Merwe mode (layer-by-layer growth) involves smooth monolayer growth under strong substrate adhesion (adhesion energy > cohesion energy) and lattice matching. The Stranski-Krastanov mode (layer-plus-island growth) begins with wetting layer(s) formation due to adhesion dominance, transitioning to three-dimensional (3D) islands as strain from lattice mismatch overcomes adhesion. The Volmer-Weber mode (island growth) features the formation of 3D islands without a wetting layer (cohesion energy > adhesion energy), common in weakly interacting systems. 11,15





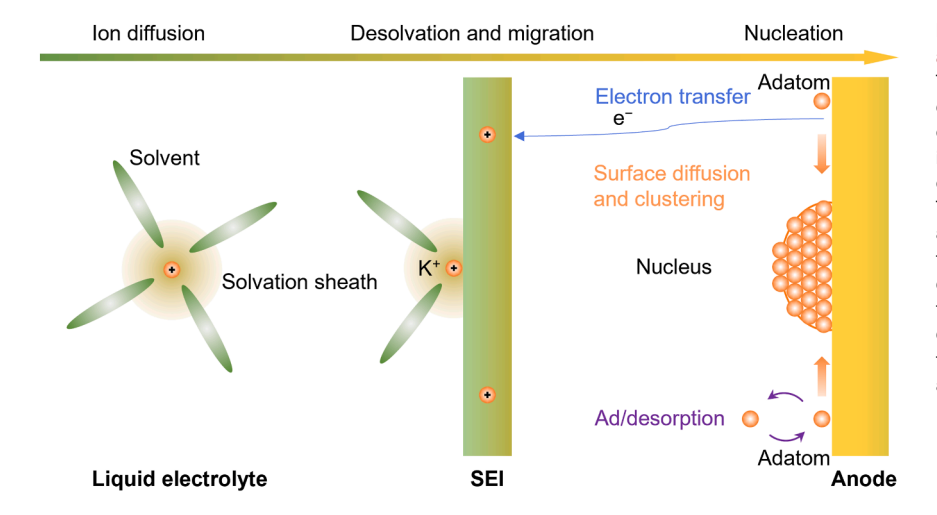


Figure 1. Schematic illustration of K nucleation during electrodeposition

The diffusion of K ions within the electrolyte is depicted, followed by their desolvation at the electrolyte/SEI interface. Subsequently, these ions traverse the SEI, acquire electrons, and emerge as adatoms at the SEI/anode interface. The adatoms then undergo surface diffusion across the anode surface, coalescing into clusters. When the clusters reach a sufficient size, they crystallize to create a nucleus that serves as the foundation for further growth. By contrast, smaller clusters lack the stability to preserve their structure and consequently disintegrate, releasing adatoms once again.

#### The framework for analyzing the K nucleation phase

The classical theory of single-component heterogeneous nucleation was first proposed by Fletcher in 1958.  $^{16,17}$  Within the framework of the capillarity approximation, the formation of a K cluster is modelled as a spherical liquid cap with radius r and contact angle  $\theta$  on a flat surface (Figure 2A; N: nucleus, E: electrolyte, S: substrate). Under the nucleation overpotential  $\eta$ , the Gibbs free energy barrier of the cluster formation ( $\Delta G_{het}$ ) is given by  $^{18-20}$ 

$$\Delta G_{het} = -\frac{4\pi}{3} r^3 F \rho_m \eta f(\theta) + 4\pi r^2 \Upsilon_{NE} f(\theta) \qquad \text{(Equation 1)}$$

where F is the Faraday constant,  $\rho_m$  is the molar density of K atoms in the cluster, and  $\Upsilon_{NE}$  denotes the nucleus (N)/electrolyte (E) interfacial energy. The shape factor  $f(\theta)$  is defined as

$$f(\theta) = \frac{(2 + \cos \theta)(1 - \cos \theta)^2}{4}$$
 (Equation 2)

The function  $f(\theta)$  increases monotonously from 0 at  $\theta=0$  to 1 at  $\theta=\pi$ . Under nonwetting conditions ( $\theta=\pi$ ), the cluster adopts a spherical shape, and the process aligns with homogeneous nucleation on metallic K. Consequently, the barrier of heterogeneous nucleation ( $0<\theta<\pi$ ) is always smaller than homogeneous nucleation barrier ( $\Delta G_{hom}$ ) under identical temperature and entropy conditions.<sup>21</sup>

The nucleation theory, having been extensively utilized in electroplating processes within aqueous solutions, has demonstrated its efficacy in elucidating the nucleation phenomena occurring in non-aqueous alkali metal batteries. <sup>22–24</sup> Of particular interest, the recent *in situ* electron microscopy observations have brought to light the formation of spherical-cap nuclei in Li electrodeposition. <sup>25</sup> It is plausible to anticipate a similar spherical-cap nucleation process for K as well. Consequently, we can confidently employ the nucleation theory as a robust analytical framework to study the nucleation and growth dynamics

within PMBs, which is expected to yield valuable insights into optimizing the electrodeposition processes for K metal anodes. **The contact angle factor** 

Equations 1 and 2 reveal that a smaller  $\theta$  corresponds to a lower  $\Delta G_{het}$ . Furthermore, as  $\theta$  increases, the growth mechanism transitions sequentially from the Frank-van der Merwe mechanism to the Stranski-Krastanov mechanism and finally to the Volmer-Weber mechanism (Figure 2B). While the precise critical values of  $\theta$  that trigger these transitions remain incompletely understood, the overall trend has been empirically validated. 13 Consequently, enhancing the wetting properties of the substrate by decreasing the contact angle of K metal has become a key strategy for realizing dendrite-free K deposition. Surface chemistry modifications, such as surface coatings, 13 functional groups, 26 and surface defects,<sup>27</sup> along with structural engineering strategies, including 3D architectures, 14 crystallographic orientation, 28 and surface roughness,<sup>29</sup> are effective approaches for designing potassiophilic substrates with low contact angles. Mitlin's group altered K wettability by using three substrates: a wettable O-functionalized carbon cloth, a non-wettable non-functionalized carbon cloth, and a Cu foil. 30 Their findings highlight the crucial role of substrate wettability in governing K nucleation, deposition morphology, and dendrite formation, as evidenced by improved potassiophilicity from a smaller contact angle with molten K. Potassiophobic substrates tend to produce spongy deposits with dendrites and nanopores, whereas potassiophilic substrates facilitate dense, pore-free deposition. Their mesoscale computational model suggests that strong K-substrate adhesion, comparable to or exceeding K-K cohesion, enhances K nucleus coverage, decreases deposit contact angle, and promotes uniform growth. This aligns with classical electrodeposition theory, where the adhesion-to-cohesion ratio governs the transition among the Frank-van der Merwe, Stranski-Krastanov, and Volmer-Weber growth modes. 15

#### The surface energy factor

Although contact angle is theoretically a suitable parameter for evaluating potassiophilicity and wettability, contact angle measurements for molten alkali metals are often considered





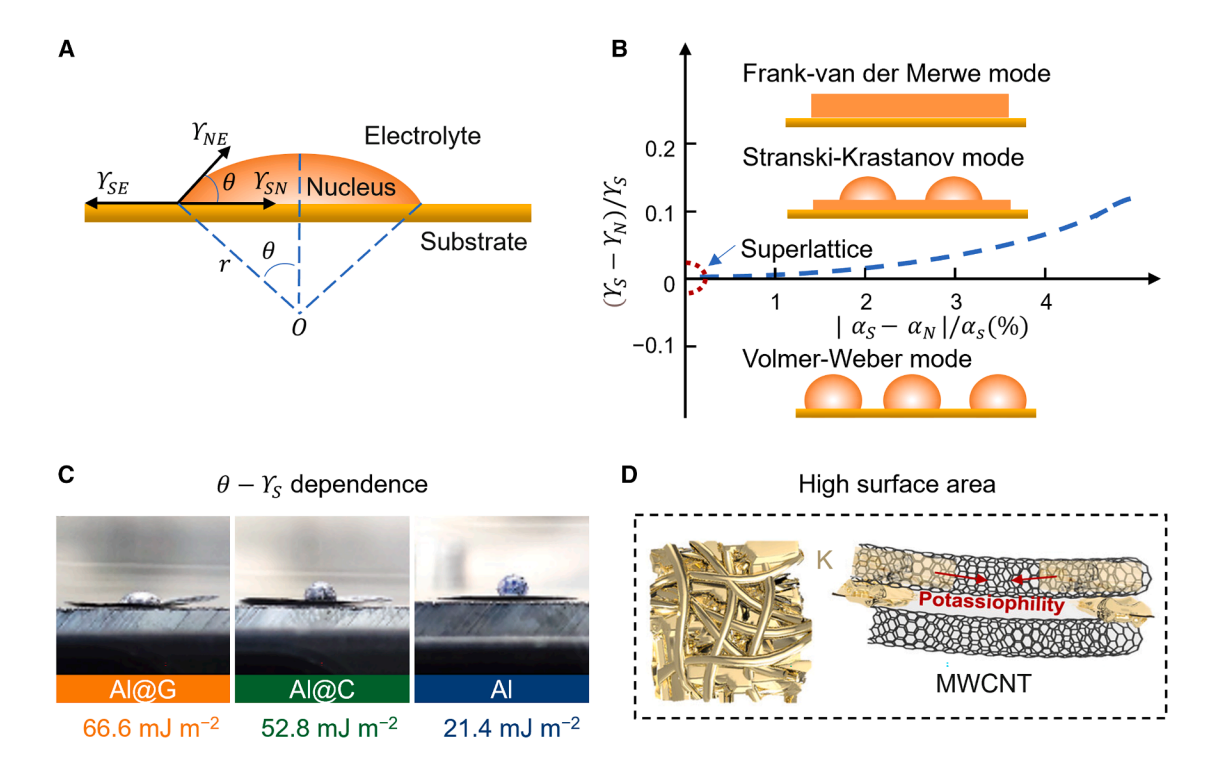


Figure 2. Thermodynamic principles of nucleation and growth

(A) Schematic of the heterogeneous nucleation model, depicting the electrolyte (E), K nucleus (N), and planar substrate (S) as distinct phases. Here,  $\theta$  donates the contact angle, and  $\Upsilon$  represents the surface or interfacial energy of the respective phases.

(B) Stability regions of growth modes, mapped in terms of the surface energy difference between the growing film and the substrate  $((\Upsilon_S - \Upsilon_N)/\Upsilon_S)$ , vertical axis) and the lattice misfit  $(|\alpha_S - \alpha_N|/\alpha_S)$ , horizontal axis). Here,  $\alpha$  represents the lattice constant. The blue dashed line in the graph delineates the transition between the Stranski-Krastanov and Volmer-Weber modes for film growth. Adapted from Wang et al. 12

(C) Experimental validation of the  $\theta - \Upsilon_S$  dependence, as observed in the wetting behavior of molten K on diverse substrates with varying surface energies. Adapted from Zhao et al. 13

(D) Diagram depicting the formation of the K/MWCNT composite anode and infiltration of K into MWCNTs. Adapted from Wang et al. 14

qualitative due to inconsistencies in experimental results. The inconsistencies primarily stem from substrate passivation layers, surface roughness, topographical discontinuities, and surface inorganics on the molten alkali metals (mainly oxides and carbonates).31 These factors, along with the temperature sensitivity of molten metal contact angles due to temperature-dependent viscosity variations, undermine their quantitative reliability, despite their widespread use in revealing general wetting trends.<sup>32</sup> Moreover, in a practical battery system, alkali metal nucleation occurs at room temperature with solid rather than liquid nuclei, leading to a contact angle that differs significantly from those of molten alkali metals.<sup>33</sup> Consequently, substrate surface energy assessment has emerged as a more practical alternative for evaluating potassiophilicity and wettability without relying on molten metal measurements. Surface energy is related to contact angle by the Young-Dupré equation:

$$\cos\theta = \frac{\Upsilon_{SE} - \Upsilon_{SN}}{\Upsilon_{NE}}$$
 (Equation 3)

where  $Y_{SE}$  and  $Y_{SN}$  represent the substrate (S)/electrolyte (E) and substrate (S)/nucleus (N) interfacial energies, respectively.

Assuming electrolytes have a negligible effect on substrates' surface energy, a substrate with a high surface energy  $Y_S$  should exhibit a low contact angle. The surface energy of air-stable substrates can be readily measured using the Owens method. 34,35 This approach involves measuring the contact angles of two liquids with known surface energies - one highly polar (e.g., water) and one nonpolar (e.g., ethylene glycol or hexadecane)-to capture diverse solid-liquid interactions. As shown in Figure 2C, Sun's group realized a potassiophilic surface of defect-rich graphene layers (130-150 nm thickness) on commercial Al foils (Al@G), with a high surface energy of 66.6 mJ m<sup>-2</sup>, surpassing carbon-coated AI foils (AI@C, 52.8 mJ m<sup>-2</sup>) and bare AI foils (21.4 mJ m<sup>-2</sup>).<sup>13</sup> The increasing substrate surface energy from bare AI to AI@C and further to AI@G correlates with the decrease in molten K contact angles, indicating strong potassiophilicity and a low  $\Delta G_{het}$  for Al@G, as described by Equations 1 and 2. This enhanced wettability, attributed to high surface energy of Al@G (Equation 3), facilitates smooth K deposition following the Frank-van der Merwe growth mode (Figure 2B) and extends plating/striping cycle stability to  $1,000 \, \text{h}$  at  $0.5 \, \text{mA} \, \text{cm}^{-2}$ . An even higher surface energy of 218.5 mJ m $^{-2}$ , 5.15 times greater than porous AI (42.4 mJ m<sup>-2</sup>), was achieved by the same group via using nitrogen-doped graphene as the modification layer on



porous Al, further improving potassiophilicity and promoting uniform K growth.<sup>36</sup>

For substrate materials with insufficient surface energy, potassiophilicity can be improved by increasing the available surface area for K nucleation, which is one of the key reasons for employing 3D host architectures. The instance, although multiwalled carbon nanotubes (MWCNTs) have a lower surface energy (28.0 mJ m $^{-2}$ ) compared with porous AI (42.4 mJ m $^{-2}$ ), the high specific surface area (92.2 m $^2$  g $^{-1}$ ) of MWCNTs compensates for this limitation (Figure 2D).  $^{14,36,38}$  Additionally, other factors contribute to their effectiveness in stabilizing K electrodeposition. MWCNTs can undergo potassiation to form potassium carbide (KC8), which significantly improves potassiophilicity by decreasing the contact angle of molten K.  $^{39,40}$  Moreover, the MWCNT matrix provides abundant K nucleation sites, accommodates volume changes, and offers high thermal stability, excellent processability, and flexibility.

It is important to note that increasing the available surface area does not necessarily require creating a rough surface, as excessive roughness can exacerbate K dendrite growth. A recent study from Lu's group demonstrated this by coating a fluorine-doped graphene oxide (F-GO) layer onto K metal foil. <sup>41</sup> This innovative coating smoothens the substrate surface while generating a uniform electric field that mitigates the "tip effect"—a phenomenon where K ions accumulate at surface protrusions, causing uneven deposition and dendrite formation. Concurrently, the porous structure of the F-GO layer increases the available surface area within its framework for K deposition. Thus, careful design of substrate surface structures is essential for realizing high surface energy without an overly rough surface.

#### Simplifying K nucleation with the binding energy factor

Building on the wettability principles established in The framework for analyzing the K nucleation phase, we now examine binding energy as a critical atomic-scale descriptor of K-substrate interactions. Nucleation is inherently site-specific and can be conceptually simplified as a series of point-to-point interactions, emphasizing the role of localized adsorption sites (Figure 3A). Binding energy quantifies the adsorption strength between K ions/atoms/clusters and specific substrate sites, making it particularly effective for analyzing materials with heterogeneous active sites such as heteroatoms, nanoparticles, or alloy phases that differ significantly from their surroundings. While surface energy and contact angle offer a macroscopic framework for nucleation thermodynamics (Equations 1-3), binding energy provides complementary atomic-scale insights into site-specific adsorption processes relevant to the early stages of nucleation, including adsorption and clustering. These active sites facilitate K-ion reduction to adatoms, lower the nucleation overpotential, and promote uniform nucleation. Effectively, binding energy also influences whether K adatoms/clusters remain anchored or diffuse across the substrate surface.

In this context, first-principles calculations serve as a powerful tool for simulating the binding energy of K ions/atoms/clusters on anode substrates. While binding energy broadly encompasses both strong interactions, such as covalent, ionic, and metallic bonds, and weaker forces, including van der Waals and hydrogen bonding, adsorption energy specifically refers to

surface interactions governed by physisorption or chemisorption. In many cases, adsorption energy and binding energy are used interchangeably, particularly when (1) a strong and stable interaction between K and the anode substrate results in a configuration with significantly lower energy than that of the non-interacting components; (2) the system consists of small entities, such as individual atoms or small molecules, where the distinction between adsorption energy and binding energy is negligible; or (3) adsorption leads to the formation of new bonds or significant modifications to existing bonds, including covalent, ionic, or metallic interactions. For clarity and consistency, the term "binding energy" will be used throughout this discussion.

#### Increasing binding energy via heteroatom doping

Porous carbon hosts with heteroatom doping strongly adsorb K atoms, enabling efficient charge transfer and ensuring uniform nucleation and growth. Using first-principles calculations, Zhang's group explored the effects of diverse heteroatom doping (B, N, O, F, P, S, Cl, Br, and I) in carbon materials on their potassiophilicity (Figure 3B).42 Their results reveal that strong adsorption arises from significant local dipoles between the doping atom and its adjacent atom, along with a critical charge transfer (Bader charge) of at least 0.89 e<sup>-</sup> from the K atom to the dopant. Based on this, the authors identified carboxylic groups (-COOH) and B-2C-O-type boron as optimal configurations for mono- and co-doping scenarios. The theoretical predictions have been extensively validated by experimental studies using O-containing groups in doped carbon substrates. 26,39,44-47 For instance, oxygen-containing functionalized porous carbon microbelts (OPCMs), synthesized via chemical exfoliation and enzyme-assisted synergy, enable K-OPCM composite anodes to achieve lower overpotential (~40 mV) and extended cycle life (over 800 h) at 1 mA cm<sup>-2</sup>, compared with bare K anodes in symmetric cells.<sup>44</sup> In addition, other heteroatom doping strategies, such as N doping, 48 P doping, 49 N/O co-doping,<sup>50</sup> N/O/S co-doping,<sup>51</sup> and amine functional groups, 52 have also shown enhancement in K electrodeposition. For example, P-doped porous carbon nanofibers infused with K, when paired with perylene-3,4,9,10-tetracarboxylic dianhydride (PTCDA) cathodes, exhibit exceptional cycling performance, achieving an 85% capacity retention after 1,000 cycles at a rate of 20 C.49

#### Increasing binding energy via inorganic nanoparticles

Beyond heteroatom doping, incorporating inorganic nanoparticles into a carbon host or applying an inorganic layer to a current collector (e.g., Cu and Al) has also shown significant promise. Inorganic materials adsorb K ions or atoms primarily through electrostatic interactions and chemical bonding (chemisorption). For instance, uniformly dispersing CoWO<sub>4</sub> nanoparticles within a honeycomb porous carbon matrix significantly enhances its potassiophilicity, increasing the binding energy of K ions on the porous carbon matrix by 3.88 times, from  $-0.57\ eV$  to  $-2.21\ eV.^{53}$ 

Several key factors must be considered when selecting inorganic nanoparticles to enhance the binding energy of the substrate or host toward K and thus improve K electrodeposition. Given the complexity of these requirements, it is challenging to find a single material that excels in all aspects; however, it is essential to excel in as many aspects as possible.





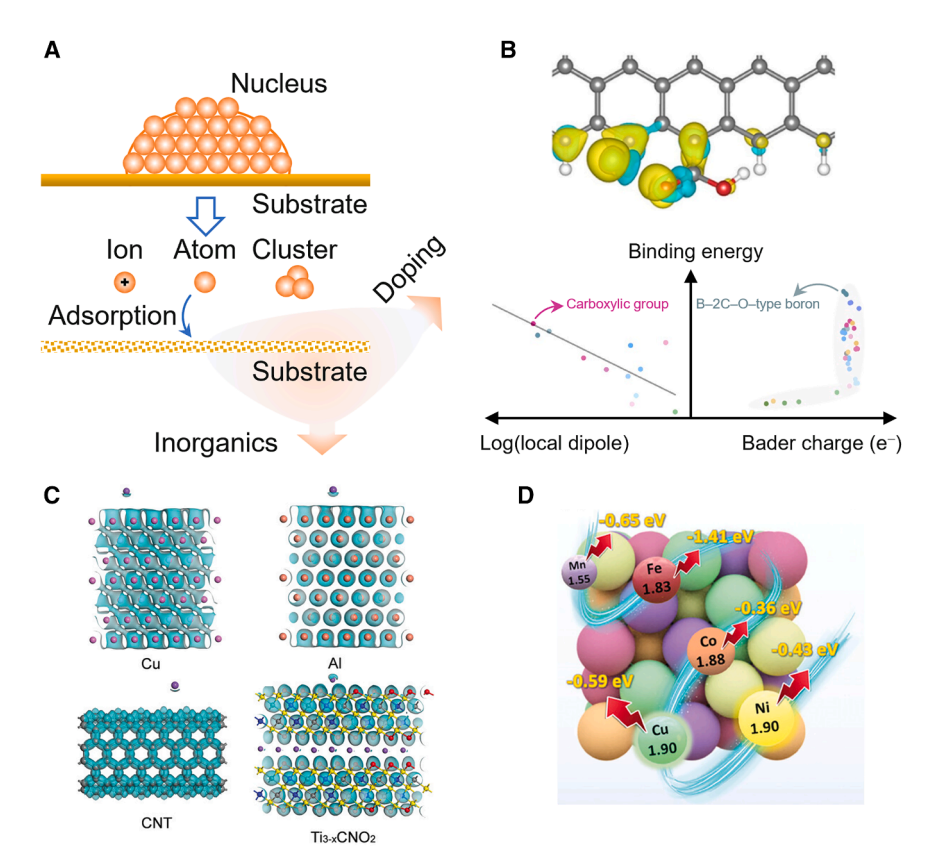


Figure 3. Principles of adsorption during nucleation

(A) Illustration of a simplified nucleation model, showcasing the adsorption of an individual ion/ atom/cluster onto the substrate surface.

(B and C) To enhance adsorption efficiency, two principal methodologies are implemented: heteroatom doping (B) and the deployment of inorganic materials (C). (B) Upper panel: a computational model based on first principles and the accompanying differential charge density for K adsorption on an oxygen-doped carbon surface featuring a carboxylic functional group. Distinct atoms are represented by varied colors: oxygen (red), hydrogen (white), and carbon (gray). Lower panel: the binding energy in correlation with local dipole and charge transfer across different doping configurations. Reproduced from Chen et al. 42 (C) DFT constructs and the resultant deformation charge density for K atoms adsorbed onto Cu, Al, CNT, and Ti<sub>3-x</sub>CNO substrates. Reproduced from Tang et al.2

(D) Comparative electronegativity values for constituent elements within an HEA. *Adapted from* Chang et al.<sup>43</sup>

- (1) Compatibility: inorganic nanoparticles should be chemically compatible with PMBs, maintaining stability under electrochemical conditions and negative potentials without significant degradation.
- (2) Structural stability: materials should retain their structural integrity during cycling, which, in some cases, directly correlates with their electrochemical stability (1).
- (3) Conductivity: highly conductive materials, including metals, <sup>54–58</sup> bimetallics, <sup>59–62</sup> and some compounds (e.g., MoC<sup>63</sup>), are beneficial to ensure efficient charge transfer and ion diffusion.
- (4) High surface area and porosity: materials such as metalorganic frameworks<sup>64</sup> and transition metal oxides<sup>65,66</sup> can offer abundant active sites for K adsorption, while their porous structures facilitate efficient K-ion diffusion.
- (5) Electrochemical activity: redox-active materials can improve K-ion adsorption and desorption during charge/ discharge cycles. Candidate materials can be drawn from electrode materials used in PIBs, such as transition metal oxides and sulfides.<sup>67</sup>

Inorganic materials with rich surface chemistries further enhance K adsorption. MXene, with its tunable composition and diverse chemical properties, has shown great potential for improving K binding energy. A defect-rich, nitrogen-containing MXene synthesized by removing Al atoms from the Ti<sub>3</sub>AlCN precursor, a process that facilitates carbon substitution by nitrogen within the MXene layers, exhibits a notable K binding energy

of -1.91 eV, which further increases to -2.27 eV with the introduction of a Ti vacancy. As shown in Figure 3C, these values significantly surpass the binding energies of Cu (-0.13 eV), Al (-0.51 eV), and CNT (-0.84 eV). The enhanced binding energy supports K nucleation, as evidenced by a substantially lower nucleation overpotential of  $\sim 6$  mV, compared with a control value exceeding 33 mV.

Intriguingly, high-entropy alloys (HEAs), composed of five or more metallic elements in near-equal or equimolar ratios, enhance K binding energy and increase the density of active nucleation sites through local electron redistribution driven by electronegativity differences (Figure 3D). 43,68 Unlike simple alloys, elemental segregation and aggregation in HEAs create alternating regions of electron accumulation and depletion within the surface layers. 69 Chemical redistribution in the surface layer, driven by the segregation of alloying atoms, can result in localized variations in surface energy at the atomic or short-range order scale. This has been demonstrated by density functional theory (DFT) calculations on equimolar face-centered cubic (FCC) AgAuCuPdPt.<sup>70</sup> The (111) surface of AgAuCuPdPt, for instance, exhibits significant segregation, with enrichment of Au and Ag and depletion of Cu, Pd, and Pt in the surface layer, resulting in a surface energy distribution that is considerably broader than that of the bulk (0.0813 eV versus 0.0317 eV per square root number of atoms). Localized high surface energies correlate with increased binding energies, thereby enhancing potassiophilicity.<sup>71</sup> Additionally, lattice distortion in HEAs raises their potential energy, further lowering the energy barrier of



adsorption.<sup>72</sup> HEAs feature an inherently complex compositional space, arising from the vast array of possible element combinations and their varying proportions. This complexity necessitates the use of high-throughput experimentation and data-driven strategies, which are well-suited for systematically tuning HEA compositions and exploring their properties in the context of K anodes.<sup>73,74</sup>

The use of binding energy to predict nucleation in K electrodeposition is a theoretical approach based on the energy released for K ions or atoms to adsorb onto the anode surface. However, this method has limitations. Unlike heterogeneous nucleation theory, which quantifies the nucleation energy barrier through thermodynamic free energy changes, the empirical correlation between high ion/atom/cluster binding energy at nucleation sites and uniform nucleation lacks a comprehensive theoretical framework. Specifically, although high binding energy has been experimentally related to low nucleation overpotential, a quantitative correlation between binding energy and the nucleation energy barrier remains undefined. By contrast, heterogeneous nucleation theory provides a well-established quantitative framework, linking the nucleation energy barrier to surface and interfacial energies (i.e., nucleus-substrate wettability) and electrochemical driving forces such as overpotential and current density. 18,23,75 Moreover, while nucleation typically initiates at the nanoscale to sub-micron scale, subsequent growth and morphological evolution extend to the micron scale. Binding energy calculations at the atomic scale may fail to capture this multiscale behavior, particularly as the binding energy per atom often varies with cluster sizes. 76 Integrating DFT with multiscale modeling frameworks is essential to bridge this gap, which will be discussed in the prospects.

#### **Combining binding energy and interfacial energy**

In The framework for analyzing the K nucleation phase, the interplay between contact angle and surface energy elucidates the K nucleation mechanism, conceptualizing the K cluster as a spherical droplet cap. Simplifying K nucleation with the binding energy factor delves into how binding energy streamlines nucleation into a sequence of localized interactions. Both models assume that the substrate's chemical properties remain predominantly unaltered, thereby preserving the K/substrate interface. If the interface is disrupted by atomic diffusion or chemical reactions, leading to the formation of a new interface for subsequent nucleation, a combined analysis of binding and interfacial energies provides valuable insights into this complex process.

This combined analysis is particularly evident in K-alloying materials, where alloying serves as a strategy to anchor K atoms to alloying seeds, optimizing binding energy to promote nucleation. However, the nucleation process remains uncertain, as binding energy primarily reflects the strength of alloying reactions rather than fully capturing K-substrate nucleation interactions; therefore, interfacial energy should be taken into consideration.

Due to alloying reactions, the K metal/alloy seed interface exhibits negative interfacial energy, leading to the formation of an intermediate alloy layer that serves as a distinct substrate for K nucleation (Figure 4A). The transition from alloying to nucleation occurs when the interfacial energy ( $Y_{IN}$ ) between the intermediate layer and K approaches zero. As per Equation 3, this

condition minimizes the contact angle, thereby enhancing potassiophilicity and lowering the nucleation energy barrier, which is favorable for stable and efficient plating/stripping cycles. The synergy between binding energy and interfacial energy is critical: strong binding energy ensures selective K deposition on alloying seeds, while decreased interfacial energy promotes a more wettable interface.

Xie's group fabricated a K host consisting of monodisperse amorphous Zn clusters embedded in hierarchically porous nitrogen-doped carbon (NC) fibers. 77 As shown in Figure 4B, DFT calculations reveal a binding energy of 2.05 eV for a K atom interacting with NC. The binding energy increases to 2.94 eV upon the introduction of a Zn cluster, demonstrating strong binding of K atoms to Zn clusters as alloying seeds. Similarly, Lu's group developed a flexible, self-supporting K host by incorporating a Bi composite into a nitrogen-doped reduced graphene oxide film (Figure 4C).<sup>78</sup> The spontaneous alloying reaction between Bi and K is driven by the strong K-Bi binding energy, which facilitates selective K deposition on Bi seeds. Simultaneously, an intermediate K-Bi alloy layer forms, decreasing interfacial energy with K and creating an ideal substrate for K nucleation with an impressively low nucleation overpotential of  $\sim$ 5 mV. This synergistic mechanism effectively suppresses dendrite growth, ensuring a stable and uniform electrodeposition process. As shown in Figure 4D, evenly distributed alloying seeds afford well-defined nucleation sites, each with a lowered nucleation energy barrier, thereby effectively directing K nucleation and alleviating the uneven deposition commonly encountered in PMBs.

Alloying seeds can be introduced through direct alloying reactions with metals such as Sn,  $^{80}$  Sb,  $^{81}$  Bi,  $^{82,83}$  Zn,  $^{77,84}$  and Hg,  $^{85}$  or indirect alloying following conversion reactions with compounds like SnS<sub>2</sub>,  $^{86}$  SnO<sub>2</sub>,  $^{87-89}$  Sb<sub>2</sub>O<sub>3</sub>,  $^{90}$  ZnO,  $^{91,92}$  and GeO<sub>2</sub>.  $^{93}$  Prior to nucleation, the formation of an intermediate alloy layer with high K affinity acts as a buffer, facilitating efficient nucleation. However, this mechanism becomes uncertain for alloy seeds with high K solubility, such as Bi, Sb, and Sn. These elements form alloys like K<sub>3</sub>Bi,  $^{94}$  K<sub>3</sub>Sb,  $^{95}$  K<sub>2</sub>Sn<sub>5</sub>, and K<sub>4</sub>Sn<sub>2</sub>3  $^{96,97}$  and are widely used as alloying-type anodes in PIBs. In such systems, intense alloying reactions may outweigh K electrodeposition, necessitating further in-depth investigation.

# THE IMPACT OF THE SEI ON K NUCLEATION AND GROWTH

The SEI is nonnegligible when investigating K electrodeposition, creating new interfaces of K/SEI and substrate/SEI besides the existing substrate/K interface. K-SEI forms more readily than Li- and Na-SEIs due to the high reducing ability of K. Contact with an electrolyte prompts the immediate formation of a chemically induced SEI on K. As PMBs start cycling, additional SEI layers are deposited, resulting from the electrochemical breakdown of the electrolyte under operating conditions. As shown in Figure 5D, SEI is a nanometer-thin layer composed of both organic and inorganic components. It acts as a critical physical barrier between the anode and the electrolyte, effectively preventing electron flow while enabling ion transport. Such dual functionality not only shields the battery from detrimental electrochemical reactions but also inhibits dendrite formation. It is





noteworthy that electron tunneling can only occur if the SEI thickness is less than 10 Å, which means the SEI discussed here is effectively electron-insulating. Of Given the essential role of the SEI as both a physical barrier and an ion transport medium, the mechanical strength and ionic conductivity of the SEI are pivotal in determining its overall effectiveness. Furthermore, the mechanical properties and ion conduction capabilities of the SEI layer are intricately linked to the nucleation behavior of K metal. Consequently, elucidating the relationships of composition-mechanical strength and composition-ionic conductivity is crucial for uncovering the underlying mechanisms that govern K electrodeposition performance.

#### Mechanical strength of the SEI

K electrodeposition subjects the SEI to mechanical pressure from the expanding K metal around the deposition sites. According to heterogeneous nucleation theory, the presence of the SEI creates new interfaces, i.e., the substrate/SEI and nucleus/SEI interfaces shown in Figure 5A instead of the substrate/electrolyte and nucleus/electrolyte interfaces shown in Figure 2A. The Young-Dupré equation is modified as follows:

$$cos\theta = \frac{Y_{SS'} - Y_{SN}}{Y_{NS'}}$$
 (Equation 4)

where S' represents the SEI layer, and  $Y_{SS'}$ ,  $Y_{SN}$ , and  $Y_{NS'}$  denote the substrate/SEI, substrate/nucleus, and nucleus/SEI interface energies, respectively.

Assuming K deforms due to a pressure difference ( $\Delta P$ ) across the nucleus/SEI interface, for a spherical-cap nucleus with orthogonal radii of surface curvature  $R_1$  and  $R_2$ ,  $\Delta P$  is given by the Laplace pressure:<sup>101</sup>

$$\Delta P = Y_{NS'}(1/R_1 + 1/R_2)$$
 (Equation 5)

For a given nucleus, Equations 4 and 5 indicate that a lower nucleus/SEI interface energy lessens the pressure difference and contact angle, indicating stronger interfacial adhesion, which stabilizes the interface. Importantly, the mechanical strength of the SEI is critical in counteracting stress, particularly during the nucleation phase when the nucleus size is small. A mechanically robust SEI resists fracture, ensuring the stability of the nucleus/SEI interface and significantly improving overall cell performance of PMBs.

Kang's group investigated how the distinct mechanical properties of SEIs on Li and K anodes influence their growth mechanisms. 
<sup>98</sup> In carbonate electrolytes, the Li-SEI, rich in Li<sub>2</sub>O and lithium ethylene dicarbonates ((CH<sub>2</sub>OCO<sub>2</sub>Li)<sub>2</sub>), exhibited enhanced strength and flexibility,  $^{102,103}$  whereas the K-SEI, deficient in K<sub>2</sub>O and dominated by alkyl carbonates (CH<sub>2</sub>ROCO<sub>2</sub>K), was more fragile. As shown in Figure 5B, the atomic force microscopy (AFM) nanoindentation force-displacement curve for Li reveals sequential elastic and plastic deformation of the SEI, followed by elastic deformation of underlying Li as displacement decreases, with a force plateau at  $\sim$ 1  $\mu$ N indicating durable plastic deformation. By contrast, a force dip at  $\sim$ 100 nN for K (Figure 5C) signifies SEI fracture under stress, highlighting the low mechanical integrity of the K-SEI. This fragility leads to cracking and fragmentation during deposition, driving distinct

K growth behavior. The robust Li-SEI directs Li growth from the root where the SEI is thinnest, forming whisker-like, anisotropic dendrites ("needles"). By contrast, the weak K-SEI fractures under local stress, exposing fresh surfaces for nucleation and resulting in isotropic, granular "forest-like" K dendrites (Figures 5B and 5C). To quantically evaluate the mechanical strength of SEI, Young's modulus (E) and elastic strain limit ( $\varepsilon_Y$ ) have been used to show the dependence of mechanical strength on SEI compositions. 104,105 As the K salt (bis(fluorosulfonyl)imide (KFSI)) concentration increased from 0.25 to 2 M, E increased while  $\varepsilon_Y$  declined, reflecting an increase in the inorganic components in the SEI (Figure 5D). As a result, a balance was reached between the two at 0.5 M to obtain the most resilient SEI, i.e., the optimal SEI strength, as an imbalance (e.g., low E at 0.25 M or low  $\varepsilon_Y$  at 2 M) can cause dendritic K growth and degrade cell performance. This is consistent with the formation of a robust Li-SEI comprising a mixed inorganic-rich and organic-rich double layer, in contrast to a less stable single inorganic-rich layer. 106

#### Ionic conductivity of the SEI

The ionic conductivity of SEIs is typically several orders of magnitude lower than that of liquid electrolytes (e.g.,  $10^{-12}$  to  $10^{-4}$  S cm<sup>-1</sup> for SEIs versus  $10^{-3}$  to  $10^{-2}$  S cm<sup>-1</sup> for liquid electrolytes). This makes ion transport through SEI the rate-limiting step in the overall process, which determines the exchange current density of the cell, highlighting the critical importance of the ionic conductivity of SEI.

Experimental studies consistently show that SEI resistance depends more on its composition than thickness, with higher inorganic content enhancing ionic conductivity. <sup>109</sup> For instance, Sun's group demonstrated the formation of an inorganic-rich SEI using a N-doped graphene-coated porous AI current collector (NG@P-AI). <sup>36</sup> The electronegativity difference between the N-doped carbon and the AI substrate reduces the electron density on AI, prioritizing electron transfer to the electrolyte salt over the solvent and thus promoting the formation of an inorganic-rich SEI. Such SEI layers exhibited significantly high ionic conductivity and low activation energy, a finding corroborated by other studies. <sup>104</sup>

Inorganic components in SEI are complex and depend on the electrolyte, while KF, K2O, and K2CO3 are the most commonly observed, with K2SO4 appearing in S-containing electrolytes. 36,110,111 Unfortunately, the ionic conductivities of these compounds in PMBs remain uncharacterized. Bond-valence energy landscape (BVEL) calculations reveal that the K diffusion energy barrier in KF is as high as 1.44 eV (Figure 5E), indicating that KF is highly ionically insulating and that ion migration through it is kinetically unfavorable, 112 evidenced by the increased charge transfer resistance of fluoroethylene carbonate (FEC)-derived KF-rich SEI. 113,114 As a result of the high K diffusion energy barrier in KF, K-ion conduction likely occurs through other, more conductive inorganic components or grain boundaries in the SEI, which is verified in lithium metal batteries, yet a hypothesis that requires further computational and experimental validation for PMBs.

To enhance the ionic conductivity of the SEI, enriching it with ion-conductive inorganic compounds has proven effective. A positive attribute is observed in  $K_2S$  and  $K_2Se$ , as both





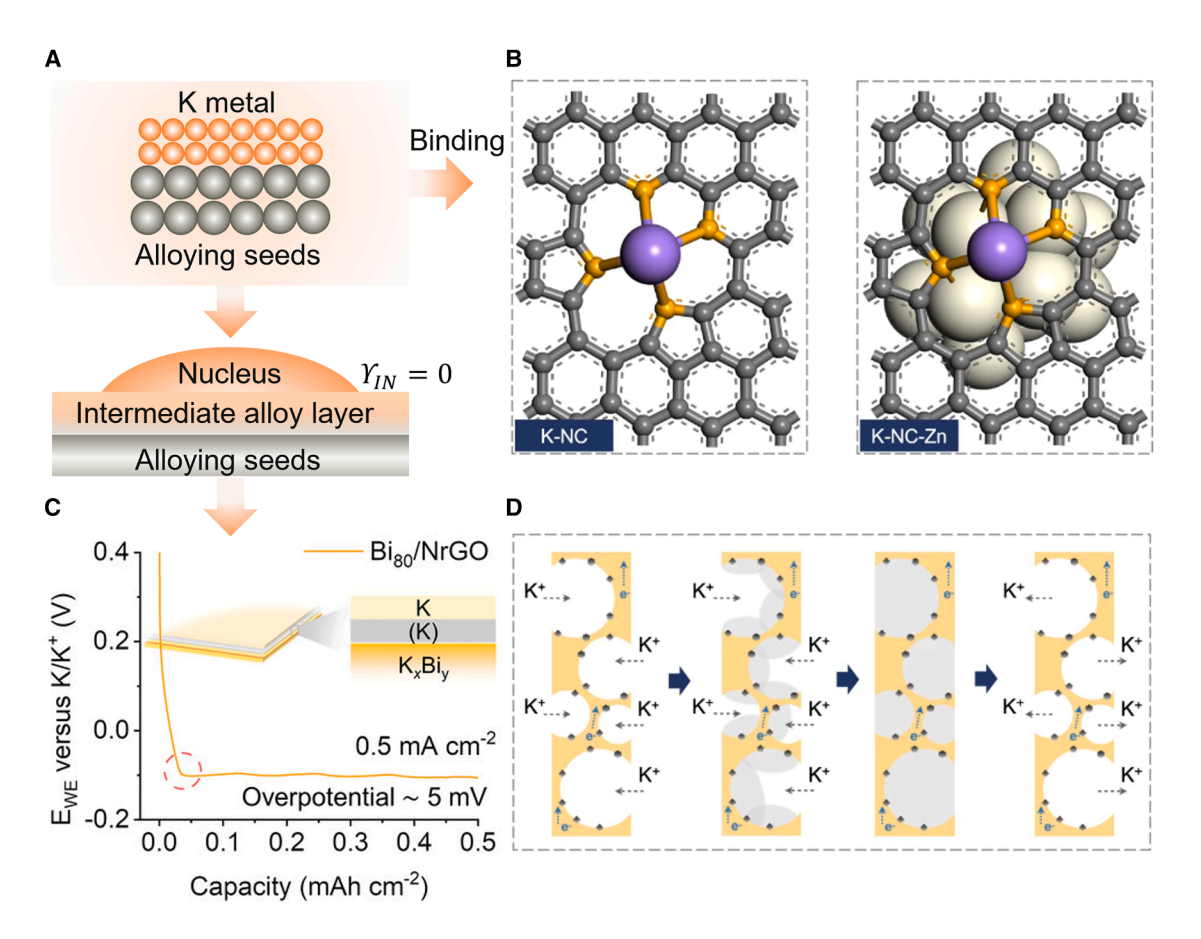


Figure 4. Integrating binding and interfacial energies in K nucleation via alloying seeds

(A) Schematic illustration of the K metal/alloying seed interface, which is conceptualized as the binding of a K atom to the seed or nucleation on an intermediate alloy layer that eliminates interfacial energy  $(Y_N)$ .

(B) DFT models depicting a K atom binding to distinct substrates. Adapted from Li et al. 77

(C) Voltage profile for K plating on a Bi<sub>80</sub>/N-doped rGO substrate at a current density of 0.5 mA cm<sup>-2</sup>, with the red dashed circle highlighting the minimal overpotential for K plating. The inset illustrates the role of the alloy buffer layer between Bi and K in lowering the nucleation barrier. *Adapted from* Feng et al.<sup>78</sup> (D) Diagram showing selective K plating and stripping on alloying seeds (dark dots) that are uniformly distributed within a porous carbon matrix (yellow structure). *Adapted from* Li et al.<sup>77</sup>

compounds demonstrate rapid K-ion migration along the [100] and [110] crystallographic directions.  $^{112,115}$  Their integration within the SEI facilitates K-ion diffusion for dendrite suppression. Moreover, Yu's group treated K metal with red phosphorus powders to form  $K_x P_y$ , which reduced the activation energy for K-ion conduction in the SEI from 70.7 kJ mol $^{-1}$  to 55.7 kJ mol $^{-1}$  and increased the exchange current density from 1.14  $\times$  10 $^{-5}$  to 3.52  $\times$  10 $^{-5}$  mA cm $^{-2}$ . $^{116}$  The enhanced ionic conductivity of the SEI decreases voltage hysteresis and significantly extends the cycle life of symmetric K||K cells from 55 to 550 h at 0.5 mA cm $^{-2}$ . They achieved similar results using tellurium (Te) powders to form  $K_2 Te$ . Ab initio molecular dynamics (AIMD) simulated trajectories of a K ion in  $K_2 Te$  reveal the [100] direction as the most favorable pathway for K-ion migration (Figure 5F).  $^{99}$ 

The SEI is dynamic rather than static. Recent *operando* AFM and X-ray photoelectron spectroscopy (XPS) studies have elucidated the morphological and compositional evolution of the Li-SEI. *Operando* AFM results revealed a two-stage SEI growth on Cu foil: a reaction-limited formation of a dense, passivating

primary layer driven by ion-coupled electron transfer, and a subsequent diffusion-limited growth of a porous secondary layer.  $^{117}$   $\it{Operando}$  XPS, performed under near-ambient pressure ( $\sim\!0.25$  mbar), confirmed the formation of  $\rm Li_2CO_3$ , lithium alkylcarbonates, and LiF, with binding energy shifts relative to potential providing indirect spatial information.  $^{118}$  Currently, the dynamic evolution of the K-SEI remains largely unexplored, particularly how its structural and compositional features influence mechanical strength and ionic conductivity, which are key factors affecting K electrodeposition. The SEI also undergoes repeated rupture and reformation during plating/stripping.  $^{119,120}$  A deeper understanding of these processes, along with the role of individual SEI components, is vital for rational interfacial design and the development of stable PMBs.

#### **SUMMARY AND PROSPECTS**

K dendrite growth remains a critical and unresolved challenge for K metal anodes, necessitating stable and long-term





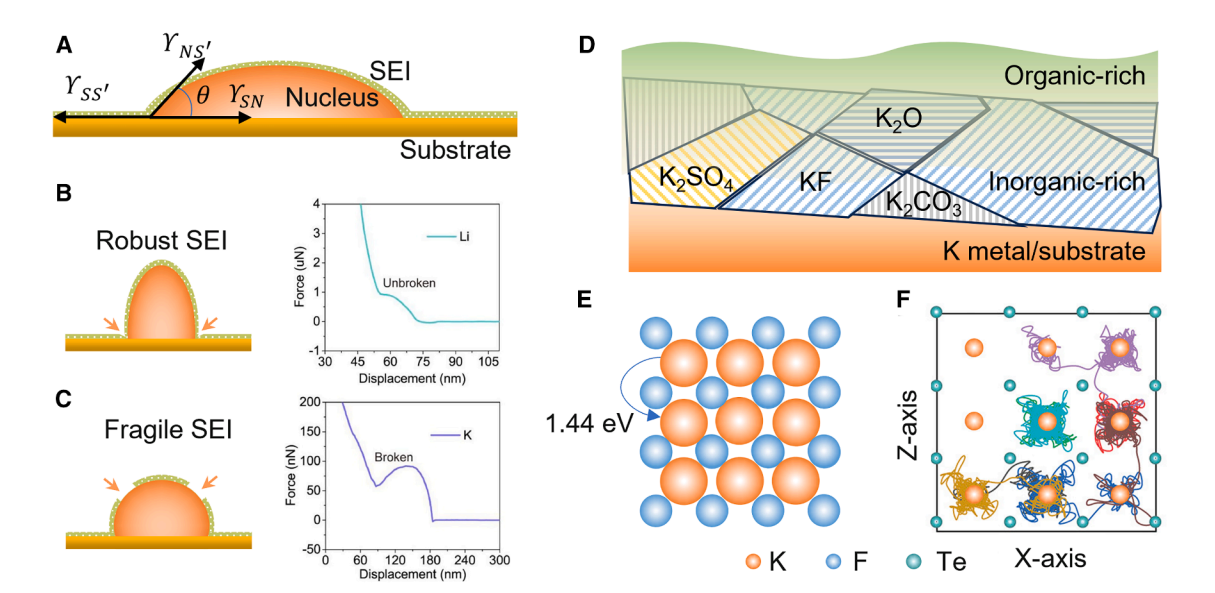


Figure 5. The impact of the SEI on K nucleation dynamics

(A) The heterogeneous nucleation model accounting for the presence of the SEI layer.

(B and C) Left: schematic depictions of the root growth mode for Li deposition and the surface growth mechanism for K deposition. Right: representative force curves obtained from AFM nanoindentation of Li and K metal foils, both covered by an SEI layer. Reproduced from Hu et al. 98

(D) Structural schematic of the SEI formed on K metal or its substrate, featuring an inorganic-rich inner layer and an organic-rich outer layer, with typical crystalline components such as KF,  $K_2O$ ,  $K_2CO_3$ , and  $K_2SO_4$ . The inorganic constituents contribute to E, while the organic components affect  $\epsilon_Y$ .

(E) An atomic-scale view of KF along the {100} plane, revealing a 1.44 eV energy barrier for K-ion migration.

(F) AIMD simulated trajectories of a K ion at 1,600 K within the X–Z plane of K<sub>2</sub>Te, with differently colored curves indicating the ion's trajectories at various lattice sites. These trajectories highlight the [100] crystal direction as the predominant migration pathway. *Reproduced from* Yang et al. <sup>99</sup>

electrodeposition to enable practical PMBs. This review presents a theoretical framework for elucidating K nucleation and early-stage growth, grounded in interfacial parameters such as contact angle, surface energy, interfacial energy, and binding energy (Figure 6). By integrating these factors, the framework offers a more nuanced perspective on the thermodynamics and kinetics of K electrodeposition. The influence of SEI is examined in parallel, with emphasis on its mechanical resilience and ionic conductivity. The structural complexity and dynamic evolution of the K-SEI, along with the evolving SEI/K and SEI/substrate interfaces, critically shape nucleation and growth behavior yet require more targeted investigation. Recent experimental advances are also reviewed, underscoring the importance of coupling theoretical insights with materials design to optimize electrodeposition behavior. Together, these insights establish a foundation for predictive, design-oriented strategies to stabilize K metal anodes and accelerate the development of high-performance, sustainable PMBs. To advance this field further, we outline key research directions (Figure 6) aimed at deepening the understanding of K electrodeposition mechanisms and SEI interfacial dynamics.

## Work of adhesion as a thermodynamic descriptor for nucleation

Existing nucleation and growth models have been instrumental in elucidating the mechanisms of K electrodeposition. However, their application has primarily been limited to simplified conditions, often neglecting the complexity introduced by SEI-related interfaces. Given the indispensable role of SEI in PMBs, both the

nucleus/SEI and substrate/SEI interfaces must be considered to accurately describe the electrodeposition process.

As discussed in this review, three interfacial energies—the nucleus/SEI, substrate/SEI, and substrate/nucleus interfacial energies—govern the contact angle and nucleation energy barrier. Work of adhesion,  $W_{adh}$ , a descriptor that integrates these interfacial energies, should be considered for K electrodeposition.  $W_{adh}$  is defined as follows:

$$W_{adh} = Y_{NS'} + Y_{SS'} - Y_{SN}$$
 (Equation 6)

This expression encapsulates the thermodynamic stability of the nucleus/substrate interface, serving as a comprehensive parameter that accounts for the overall interfacial energies involved in its formation or dissociation. A high  $W_{adh}$  corresponds to a more stable interface and a lower contact angle  $\theta$ , arising from high nucleus/SEI and substrate/SEI interfacial energies and low substrate/nucleus interfacial energy. As a result,  $W_{adh}$  can be seen as a robust descriptor of the K nucleation process, providing design guidance for substrates, SEIs, and artificial SEIs. For example, substrates with a high  $W_{adh}$  and large accessible surface areas are expected to enhance thermodynamic stability and reduce the nucleation barrier, thereby enabling more uniform K deposition.

#### Electrolyte engineering to optimize the SEI

Electrolyte engineering is central in tailoring SEI composition to achieve uniform, ionically conductive, and mechanically robust interphases. As salt concentration increases in the electrolyte, ion





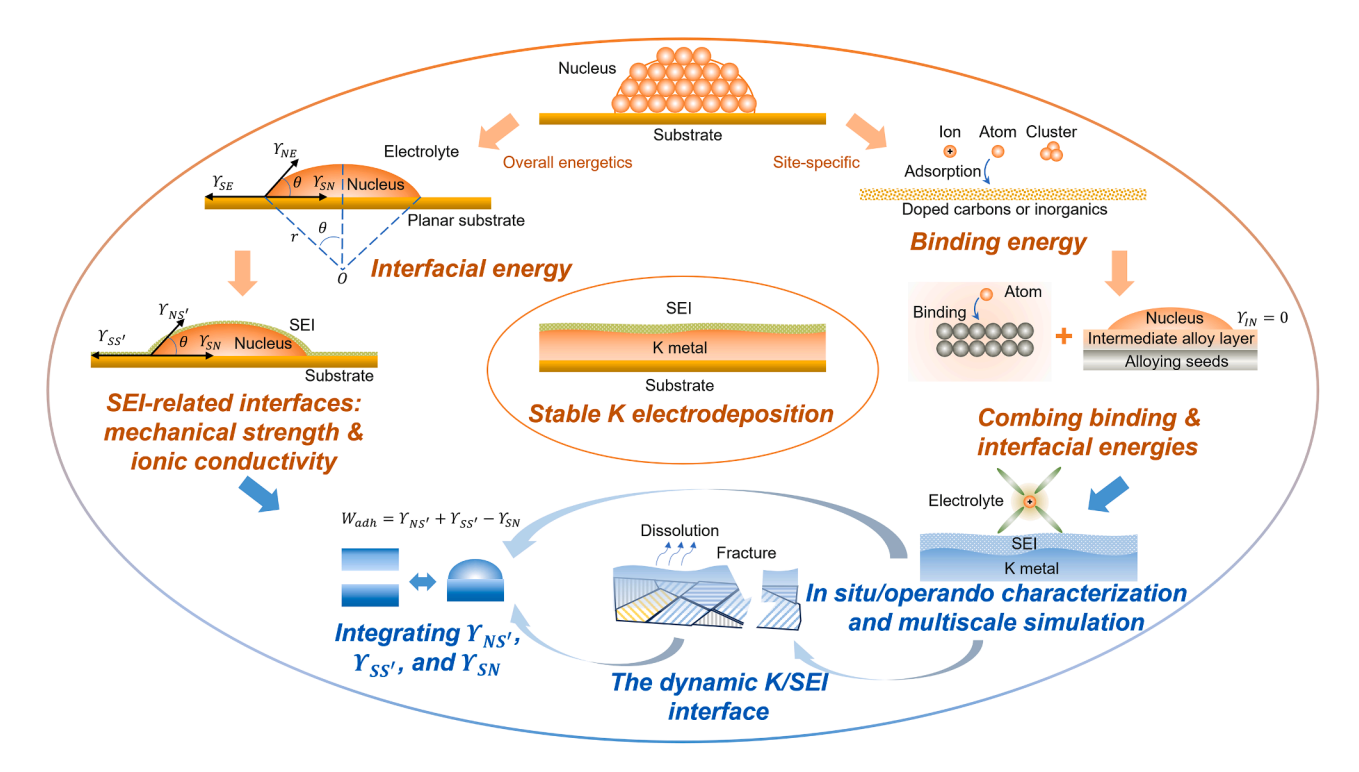


Figure 6. Key factors and future directions for stable K electrodeposition

A schematic overview highlighting the key factors for achieving stable K electrodeposition and future research directions. The crucial factors include energetic parameters such as interfacial energy, binding energy, and their combined effects, along with the mechanical strength and ionic conductivity of the SEI. Future research directions encompass leveraging work of adhesion for optimized substrate design, exploring the dynamic evolution of the K/SEI interface and its impact on K electrodeposition, and gaining deeper experimental insights.

pair structures evolve from solvent-separated ion pairs (SSIPs) to contact ion pairs (CIPs) and ultimately to aggregates (AGGs), depending on the number of cations coordinated with each anion. 121 This progression reduces free solvent availability and reshapes the solvation environment. In high-concentration electrolytes (HCEs), dense ion clustering broadens the electrochemical stability window and favors the formation of inorganic-rich, stable SEI layers. Localized high-concentration electrolytes (LHCEs), which incorporate non-solvating diluents, preserve the beneficial solvation characteristics of HCEs while alleviating drawbacks such as high viscosity, thereby offering a balanced approach to interfacial stability and processability. 100 Further modulation of ion cluster size and packing density can enhance anion reduction kinetics and ion mobility, facilitating the formation of ultrathin, uniform SEI layers and suppressing dendrite growth. Recent studies in lithium electrolytes demonstrate that larger ion AGGs (~3–4 nm) accelerate anion reduction and yield thin, inorganic-rich SEIs, 122 whereas smaller clusters improve ionic conductivity and foster uniform metal deposition. 123 Optimized solvation structures comprising compact anion-Li+ complexes of intermediate size exhibit high ionic conductivity, low desolvation barriers, and homogeneous inorganic SEI components, underscoring the strong interplay between solvation structure and interfacial stability. 124 These results may serve as "drop-in" strategies for engineering K electrolytes and SEIs; however, caution is warranted when comparing Li and K systems, as elucidating their fundamental differences offers greater insights than merely identifying transferable approaches. Advancing the strategies of electrolyte and SEI optimization requires integrating computational modeling, *in situ/operando* characterization, and multifunctional electrolyte design. Ultimately, interdisciplinary approaches that unify solvation engineering, interfacial chemistry, and mechanical durability will be essential for achieving high-energy-density, long-cycle-life PMBs.

#### In situ/operando characterization of the anode

Despite the critical role of the SEI in K electrodeposition, it remains poorly understood due to its compositional and structural complexities, along with its dynamic evolution during cyclingoften driven by instability and inhomogeneity. 126,127 A complete understanding of SEIs and their influences on K electrodeposition requires precise characterization of their structural, chemical, mechanical, and dynamic features. In situ and operando techniques are particularly valuable, as they enable real-time observation of interfacial processes while avoiding artifacts caused by air exposure, salt precipitation, or the dissolution of semi-soluble layers during post-treatment. 117 Although still limited in PMB research, recent studies in Li and Na systems offer important methodological guidance. 128 A range of advanced in situ/operando tools can be employed to probe K electrodeposition, SEI evolution, and interfacial dynamics: (cryo-)electron microscopy for nanostructure and elemental





mapping,<sup>129</sup> AFM for surface morphology and mechanical properties,<sup>117</sup> laser scanning confocal microscopy (LSCM) for dendrite evolution and interfacial dynamics,<sup>130</sup> X-ray microscopy for 3D defect visualization,<sup>131</sup> XPS for surface chemical state analysis,<sup>118</sup> time-of-flight secondary ion mass spectrometry (ToF-SIMS) for molecular-level heterogeneity,<sup>132</sup> nuclear magnetic resonance (NMR) for ion transport and solvation behavior,<sup>133</sup> and depth-sensitive plasmon-enhanced Raman spectroscopy (DS-PERS) for nanostructural and bonding depth profiling.<sup>134</sup> The integration of these techniques will be essential for elucidating the SEI's chemical composition, mechanical properties, and ionic conductivity and for establishing quantitative relationships among these characteristics and the complex interfacial phenomena that govern K electrodeposition, thereby guiding the design of stable, high-performance K metal anodes.

#### **Multiscale simulation frameworks**

Complementing advanced characterization, multiscale simulation frameworks that integrate DFT, molecular dynamics (MD), and phase-field simulations are essential for elucidating the complex processes governing K nucleation and growth. MD simulations offer insights into nanoscale K cluster formation and growth dynamics under realistic electrochemical conditions, while phase-field models incorporating interfacial energy, overpotential, and concentration gradients capture mesoscale morphology evolution, such as dendrite propagation or compact layer formation. These modeling approaches have been successfully applied to Li and Na metal systems to bridge atomicscale energetics with macroscopic deposition behavior. 135-138 However, K metal anodes pose unique challenges due to their larger ionic radius and higher chemical reactivity compared with Li/Na, potentially altering nucleation kinetics and interfacial stability. Future efforts should prioritize these multiscale strategies, explicitly incorporating electrochemical parameters, such as overpotential-dependent nucleation rates and electrolyte concentration effects, to refine K nucleation theory and inform substrate design for uniform deposition. 139

Filling these knowledge and methodological gaps will be extremely valuable for developing a more predictive and rational approach to stabilize K metal anodes, ultimately accelerating the practical realization of PMBs. In the short term, research should prioritize achieving stable and reversible K plating/stripping through strategic interfacial engineering, substrate design, and electrolyte optimization. Long-term efforts should aim to integrate K metal anodes with high-performance cathodes to enhance cell-level energy density and cycle life. The ultimate objective is to develop full-cell architectures that combine high energy density, extended cycling stability, and scalable manufacturing compatibility, thereby advancing the commercialization of next-generation PMBs for grid-scale energy storage and other demanding applications.

#### **ACKNOWLEDGMENTS**

Y.X. acknowledges the support of the Engineering and Physical Sciences Research Council (EP/X000087/1), the Leverhulme Trust (RPG-2021-138 and RPG-2025-127), and the Royal Society (IEC\NSFC\223016). Y.H. acknowledges the support from the China Scholarship Council (CSC). For the

purpose of open access, the authors have applied a Creative Commons Attribution (CC BY) license to any author accepted manuscript version arising.

#### **AUTHOR CONTRIBUTIONS**

Conceptualization, Y.H. and Y.X.; formal analysis, Y.H. and P.H.; investigation, Y.H. and P.H.; funding acquisition, Y.X.; supervision, Y.X.; validation, Y.H. and P.H.; visualization, Y.H.; writing – original draft, Y.H.; writing – review & editing, Y.H., P.H., and Y.X.

#### **DECLARATION OF INTERESTS**

The authors declare no competing interests.

#### **REFERENCES**

- Liu, D.-H., Bai, Z., Li, M., Yu, A., Luo, D., Liu, W., Yang, L., Lu, J., Amine, K., and Chen, Z. (2020). Developing high safety Li-metal anodes for future high-energy Li-metal batteries: strategies and perspectives. Chem. Soc. Rev. 49, 5407–5445. https://doi.org/10.1039/C9CS00636B.
- Wang, H., Matios, E., Luo, J., and Li, W. (2020). Combining theories and experiments to understand the sodium nucleation behavior towards safe sodium metal batteries. Chem. Soc. Rev. 49, 3783–3805. https://doi.org/ 10.1039/D0CS00033G.
- Liu, P., and Mitlin, D. (2020). Emerging Potassium Metal Anodes: Perspectives on Control of the Electrochemical Interfaces. Acc. Chem. Res. 53, 1161–1175. https://doi.org/10.1021/acs.accounts.0c00099.
- Zhou, M., Bai, P., Ji, X., Yang, J., Wang, C., and Xu, Y. (2021). Electrolytes and Interphases in Potassium Ion Batteries. Adv. Mater. 33, e2003741. https://doi.org/10.1002/adma.202003741.
- Xu, Y., Du, Y., Chen, H., Chen, J., Ding, T., Sun, D., Ha Kim, D.H., Lin, Z., and Zhou, X. (2024). Recent advances in rational design for high-performance potassium-ion batteries. Chem. Soc. Rev. 53, 7202–7298. https:// doi.org/10.1039/D3CS00601H.
- Liu, S., Kang, L., and Jun, S.C. (2021). Challenges and Strategies toward Cathode Materials for Rechargeable Potassium-Ion Batteries. Adv. Mater. 33, e2004689. https://doi.org/10.1002/adma.202004689.
- Liu, W., Liu, P., and Mitlin, D. (2020). Review of Emerging Concepts in SEI Analysis and Artificial SEI Membranes for Lithium, Sodium, and Potassium Metal Battery Anodes. Adv. Energy Mater. 10, 2002297. https:// doi.org/10.1002/aenm.202002297.
- Tang, M., Dong, S., Wang, J., Cheng, L., Zhu, Q., Li, Y., Yang, X., Guo, L., and Wang, H. (2023). Low-temperature anode-free potassium metal batteries. Nat. Commun. 14, 6006. https://doi.org/10.1038/s41467-023-41778-6.
- Chen, J., Lan, H., Wang, S., Liu, X., Zhu, Q., Zhang, X., Tang, M., Dong, S., Yang, J., Kurbanov, M., et al. (2025). Realizing an Energy-Dense Potassium Metal Battery at –40 °C via an Integrated Anode-Free and Duallon Strategy. J. Am. Chem. Soc. 147, 2393–2402. https://doi.org/10. 1021/jacs.4c12126.
- Cooper, E.R., Li, M., Gentle, I., Xia, Q., and Knibbe, R. (2023). A Deeper Understanding of Metal Nucleation and Growth in Rechargeable Metal Batteries Through Theory and Experiment. Angew. Chem. Int. Ed. Engl. 62, e202309247. https://doi.org/10.1002/anie.202309247.
- Kanani, N. (2004). Electrodeposition Considered at the Atomistic Level-Chapter 5. In Electroplating, N. Kanani, ed. (Elsevier), pp. 141–177. https://doi.org/10.1016/B978-185617451-0/50005-1.
- Wang, D., Zhang, W., Zheng, W., Cui, X., Rojo, T., and Zhang, Q. (2017).
   Towards High-Safe Lithium Metal Anodes: Suppressing Lithium Dendrites via Tuning Surface Energy. Adv. Sci. (Weinh) 4, 1600168. https://doi.org/10.1002/advs.201600168.
- Zhao, Y., Liu, B., Yi, Y., Lian, X., Wang, M., Li, S., Yang, X., and Sun, J. (2022). An Anode-Free Potassium-Metal Battery Enabled by a Directly



- Grown Graphene-Modulated Aluminum Current Collector. Adv. Mater. 34, e2202902. https://doi.org/10.1002/adma.202202902.
- Wang, Z., Wu, J.-F., Zhou, W., Mo, Y., Chen, S., Zhou, T., Shen, W., Ren, B., Huang, P., and Liu, J. (2024). Ultrathin K–C Composite Anode Enables Conformal Stripping/Plating for Dendrite-Free and High-Rate Potassium-Metal Batteries. ACS Energy Lett. 9, 4534–4543. https://doi.org/10.1021/ acsenergylett.4c01982.
- Budevski, E.B., Staikov, G.T., and Lorenz, W.J. (2008). Electrochemical Phase Formation and Growth: an Introduction to the Initial Stages of Metal Deposition (John Wiley & Sons).
- Fletcher, N.H. (1958). Size Effect in Heterogeneous Nucleation. J. Chem. Phys. 29, 572–576. https://doi.org/10.1063/1.1744540.
- Kalikmanov, V.I. (2013). Classical Nucleation Theory. In Nucleation Theory, V.I. Kalikmanov, ed. (Springer Netherlands), pp. 17–41. https://doi.org/10.1007/978-90-481-3643-8\_3.
- Ely, D.R., and García, R.E. (2013). Heterogeneous Nucleation and Growth of Lithium Electrodeposits on Negative Electrodes.
   J. Electrochem. Soc. 160, A662–A668. https://doi.org/10.1149/1. 057304jes.
- Winter, D., Virnau, P., and Binder, K. (2009). Monte Carlo Test of the Classical Theory for Heterogeneous Nucleation Barriers. Phys. Rev. Lett. 103, 225703. https://doi.org/10.1103/PhysRevLett.103.225703.
- W. Plieth, ed. (2008). Electrochemistry for Materials Science, First Edition (Flsevier)
- Kalikmanov, V.I. (2013). Heterogeneous Nucleation. In Nucleation Theory, V.I. Kalikmanov, ed. (Springer Netherlands), pp. 253–276. https://doi.org/10.1007/978-90-481-3643-8 15.
- Kanani, N. (2004). Materials that can be ElectroplatedChapter 2. In Electroplating, N. Kanani, ed. (Elsevier), pp. 21–53. https://doi.org/10.1016/B978-185617451-0/50002-6.
- Pei, A., Zheng, G., Shi, F., Li, Y., and Cui, Y. (2017). Nanoscale Nucleation and Growth of Electrodeposited Lithium Metal. Nano Lett. 17, 1132– 1139. https://doi.org/10.1021/acs.nanolett.6b04755.
- Huang, F., Xu, P., Fang, G., and Liang, S. (2024). In-Depth Understanding of Interfacial Na+ Behaviors in Sodium Metal Anode: Migration, Desolvation, and Deposition. Adv. Mater. 36, e2405310. https://doi.org/10.1002/ adma.202405310.
- Wang, C., Wang, H., Tao, L., Wang, X., Cao, P., Lin, F., and Xin, H.L. (2023). Direct Observation of Nucleation and Growth Behaviors of Lithium by In Situ Electron Microscopy. ACS Energy Lett. 8, 1929–1935. https://doi.org/10.1021/acsenergylett.3c00180.
- Liu, P., Wang, Y., Gu, Q., Nanda, J., Watt, J., and Mitlin, D. (2020).
   Dendrite-Free Potassium Metal Anodes in a Carbonate Electrolyte.
   Adv. Mater. 32, e1906735. https://doi.org/10.1002/adma.201906735.
- Tang, X., Zhou, D., Li, P., Guo, X., Sun, B., Liu, H., Yan, K., Gogotsi, Y., and Wang, G. (2020). MXene-Based Dendrite-Free Potassium Metal Batteries. Adv. Mater. 32, e1906739. https://doi.org/10.1002/adma. 201906739.
- Tang, F., Yang, Y., Liu, C., Yang, S., Xu, S., Yao, Y., Yang, H., Yang, Y., He, S., Pan, H., et al. (2025). Initially anode-free sodium metal battery enabled by strain-engineered single-crystal aluminum substrate with (100)-preferred orientation. Nat. Commun. 16, 2280. https://doi.org/10. 1038/s41467-025-57424-2.
- Liu, P., Wang, Y., Hao, H., Basu, S., Feng, X., Xu, Y., Boscoboinik, J.A., Nanda, J., Watt, J., and Mitlin, D. (2020). Stable Potassium Metal Anodes with an All-Aluminum Current Collector through Improved Electrolyte Wetting. Adv. Mater. 32, e2002908. https://doi.org/10.1002/adma. 202002908.
- Liu, P., Yen, D., Vishnugopi, B.S., Kankanallu, V.R., Gürsoy, D., Ge, M., Watt, J., Mukherjee, P.P., Chen-Wiegart, Y.K., and Mitlin, D. (2023). Influence of Potassium Metal-Support Interactions on Dendrite Growth. Angew. Chem. Int. Ed. Engl. 62, e202300943. https://doi.org/10.1002/anie.202300943.

- Wang, J., Wang, H., Xie, J., Yang, A., Pei, A., Wu, C.-L., Shi, F., Liu, Y., Lin, D., Gong, Y., et al. (2018). Fundamental study on the wetting property of liquid lithium. Energy Storage Mater. 14, 345–350. https://doi.org/10. 1016/j.ensm.2018.05.021.
- Krat, S.A., Popkov, A.S., Gasparyan, Yu.M., Pisarev, A.A., Fiflis, P., Szott, M., Christenson, M., Kalathiparambil, K., and Ruzic, D.N. (2017). Wetting properties of liquid lithium on lithium compounds. Fusion Eng. Des. 117, 199–203. https://doi.org/10.1016/j.fusengdes.2016.06.038.
- Zhu, S., Xie, K., Lin, Q., Cao, R., and Qiu, F. (2023). Experimental determination of surface energy for high-energy surface: A review. Adv. Colloid Interface Sci. 315, 102905. https://doi.org/10.1016/j.cis.2023. 102905.
- Kozbial, A., Li, Z., Conaway, C., McGinley, R., Dhingra, S., Vahdat, V., Zhou, F., D'Urso, B., Liu, H., and Li, L. (2014). Study on the Surface Energy of Graphene by Contact Angle Measurements. Langmuir 30, 8598–8606. https://doi.org/10.1021/la5018328.
- Owens, D.K., and Wendt, R.C. (1969). Estimation of the surface free energy of polymers. J. Appl. Polym. Sci. 13, 1741–1747. https://doi.org/10.1002/app.1969.070130815.
- Lian, X., Ju, Z., Li, L., Yi, Y., Zhou, J., Chen, Z., Zhao, Y., Tian, Z., Su, Y., Xue, Z., et al. (2024). Dendrite-Free and High-Rate Potassium Metal Batteries Sustained by an Inorganic-Rich SEI. Adv. Mater. 36, e2306992. https://doi.org/10.1002/adma.202306992.
- Wang, J., Yan, W., and Zhang, J. (2022). High area capacity and dendritefree anode constructed by highly potassiophilic Pd/Cu current collector for low-temperature potassium metal battery. Nano Energy 96, 107131. https://doi.org/10.1016/j.nanoen.2022.107131.
- Al-Saleh, M.H. (2019). Measuring surface energy of carbon nanotubes using modified washburn method. Mater. Res. Express 6, 115088. https://doi.org/10.1088/2053-1591/ab4b2c.
- Yang, Y., Huang, C., Zhang, Y., Wu, Y., Zhao, X., Qian, Y., Chang, G., Tang, Q., Hu, A., and Chen, X. (2022). Processable Potassium–Carbon Nanotube Film with a Three-Dimensional Structure for Ultrastable Metallic Potassium Anodes. ACS Appl. Mater. Interfaces 14, 55577– 55586. https://doi.org/10.1021/acsami.2c16255.
- Lei, Y., Zhang, S., Dong, J., Gao, Y., Gao, C., Wei, Y., Qin, L., Han, D., Huang, D., Wei, G., et al. (2023). Potassium-enriched graphite for use as stable hybrid anodes in high-efficiency potassium batteries. Carbon 201, 1030–1037. https://doi.org/10.1016/j.carbon.2022.09.088.
- Ding, H., Wang, J., Zhou, J., Wang, C., and Lu, B. (2023). Building electrode skins for ultra-stable potassium metal batteries. Nat. Commun. 14, 2305. https://doi.org/10.1038/s41467-023-38065-9.
- Chen, X., Bai, Y.-K., Shen, X., Peng, H.-J., and Zhang, Q. (2020). Sodiophilicity/potassiophilicity chemistry in sodium/potassium metal anodes. J. Energy Chem. 51, 1–6. https://doi.org/10.1016/j.jechem.2020.03.051.
- Chang, C.B., Tseng, Y.Y., Lu, Y.R., Yang, Y.C., and Tuan, H.Y. (2024).
   High Entropy Induced Local Charge Enhancement Promotes Frank-Van der Merwe Growth for Dendrite-Free Potassium Metal Batteries.
   Adv. Funct. Mater. 34, 2411193. https://doi.org/10.1002/adfm. 202411193.
- 44. Xie, S., Xie, W., Zhang, Q., Cheng, X., Ouyang, X., and Lu, B. (2023). Structure-Engineered Low-Cost Carbon Microbelt Hosts for Highly Robust Potassium Metal Anode. Adv. Funct. Mater. 33, 2302880. https://doi.org/10.1002/adfm.202302880.
- Li, Z., Ma, L., Han, K., Ji, Y., Xie, J., Pan, L., Li, J., and Mai, W. (2023). A host potassiophilicity strategy for unprecedentedly stable and safe K metal batteries. Chem. Sci. 14, 9114–9122. https://doi.org/10.1039/ D3SC03203E.
- Sun, J., Duan, L., Yuan, Z., Li, X., Yan, D., and Zhou, X. (2024). Hydroxyl-Decorated Carbon Cloth with High Potassium Affinity Enables Stable Potassium Metal Anodes. Small 20, e2311314. https://doi.org/10.1002/ smll.202311314.





- Zhou, M., Qi, W., Hu, Z., Cheng, M., Zhao, X., Xiong, P., Su, H., Li, M., Hu, J., and Xu, Y. (2021). Highly Potassiophilic Carbon Nanofiber Paper Derived from Bacterial Cellulose Enables Ultra-Stable Dendrite-Free Potassium Metal Anodes. ACS Appl. Mater. Interfaces 13, 17629–17638. https://doi.org/10.1021/acsami.1c02186.
- Xiong, J., Ye, M., Wang, Z., Chen, J., Zhang, Y., Tang, Y., and Li, C.C. (2022). Fast and homogeneous ion regulation toward a 4 V, high rate and dendrite-free potassium metal battery. Chem. Eng. J. 442, 135927. https://doi.org/10.1016/j.cej.2022.135927.
- Chen, Z., Wang, L., Zheng, J., Huang, Y., Huang, H., Li, C., Shao, Y., Wu, X., Rui, X., Tao, X., et al. (2024). Unraveling the Nucleation and Growth Mechanism of Potassium Metal on 3D Skeletons for Dendrite-Free Potassium Metal Batteries. ACS Nano 18, 8496–8510. https://doi.org/10.1021/acsnano.4c00881.
- Zhao, L.K., Gao, X.W., Mu, J., Luo, W.B., Liu, Z., Sun, Z., Gu, Q.F., and Li, F. (2023). Durable Integrated K-Metal Anode with Enhanced Mass Transport through Potassiphilic Porous Interconnected Mediator. Adv. Funct. Mater. 33, 2304292. https://doi.org/10.1002/adfm.202304292.
- Shen, X., Sun, H., Li, B., Yuan, Y., Zhang, L., Li, S., Wang, L., Lu, B., Zhu, J., and Duan, X. (2023). Dual-strategy coupling driven versatile carbonbased anode for potassium-ion/potassium metal storage. Chem. Eng. J. 473, 145155. https://doi.org/10.1016/j.cej.2023.145155.
- Meng, J., Zhu, H., Xiao, Z., Zhang, X., Niu, C., Liu, Y., Jiang, G., Wang, X., Qiao, F., Hong, X., et al. (2022). Amine-Wetting-Enabled Dendrite-Free Potassium Metal Anode. ACS Nano 16, 7291–7300. https://doi.org/10. 1021/acsnano.2c01432.
- Song, L., Li, R., Liao, W., Sun, J., Li, X., Xu, Y., Zhou, G., and Zhou, X. (2024). A flexible and potassiphilic porous interconnected mediator for dendrite-free and stable potassium metal anodes. Energy Storage Mater. 71, 103643. https://doi.org/10.1016/j.ensm.2024.103643.
- 54. Yi, Y., Li, J., Gao, Z., Liu, W., Zhao, Y., Wang, M., Zhao, W., Han, Y., Sun, J., and Zhang, J. (2022). Highly Potassiophilic Graphdiyne Skeletons Decorated with Cu Quantum Dots Enable Dendrite-Free Potassium-Metal Anodes. Adv. Mater. 34, e2202685. https://doi.org/10.1002/adma.202202685.
- Zhang, J., Li, Y., Zhu, L., Wang, X., and Tu, J. (2022). Potassiophilic skeleton achieving highly stable potassium metal anode. Chem. Eng. J. 449, 137659. https://doi.org/10.1016/j.cej.2022.137659.
- Zhang, J., Cai, D., Zhu, L., Wang, X., and Tu, J. (2023). Highly Stable Potassium Metal Anodes with Controllable Thickness and Area Capacity. Small 19, e2301119. https://doi.org/10.1002/smll.202301119.
- Zhang, D., Ma, X., Wu, L., Wen, J., Li, F., Zhou, J., Rao, A.M., and Lu, B. (2023). Coupling Low-Tortuosity Carbon Matrix with Single-Atom Chemistry Enables Dendrite-Free Potassium-Metal Anode. Adv. Energy Mater. 13, 2203277. https://doi.org/10.1002/aenm.202203277.
- Wang, L., Wang, H., Cheng, M., Hong, Y., Li, M., Su, H., Sun, J., Wang, J., and Xu, Y. (2021). Metal–Organic Framework@Polyacrylonitrile-Derived Potassiophilic Nanoporous Carbon Nanofiber Paper Enables Stable Potassium Metal Anodes. ACS Appl. Energy Mater. 4, 6245–6252. https://doi.org/10.1021/acsaem.1c01002.
- Wang, J., Yuan, J., Chen, C., Wang, L., Zhai, Z., Fu, Q., Liu, Y., Dong, L., Yan, W., Li, A., et al. (2020). Cu3Pt alloy-functionalized Cu mesh as current collector for dendritic-free anodes of potassium metal batteries. Nano Energy 75, 104914. https://doi.org/10.1016/j.nanoen.2020. 104914.
- Ren, N., Wang, L., Li, X., Cao, K., He, Z., Shao, Y., Xiao, J., Zhu, Y., Pan, B., Jiao, S., et al. (2024). Design Principles of Mediation Layer for Current Collectors Toward High-Performance Anode-Free Potassium-Metal Batteries: A Case Study of Cu<sub>6</sub> Sn<sub>5</sub> on Copper. Adv. Funct. Mater. 34, 2313538. https://doi.org/10.1002/adfm.202313538.
- Cheng, G., Liu, S., Wang, X., Li, X., Su, Y., Shi, J., Huang, M., Shi, Z., Wang, H., and Yan, Z. (2022). CoZn Nanoparticles@Hollow Carbon Tubes Enabled High-Performance Potassium Metal Batteries. ACS

- Appl. Mater. Interfaces 14, 45364–45372. https://doi.org/10.1021/acsami.2c12058.
- Shen, Q., He, Y., and Wang, J. (2023). Biomass-derived two-dimensional N,O-doped carbon with embedded binary-metal nanoparticles enables dendrite-free potassium-metal anodes. J. Mater. Chem. A 11, 9829– 9839. https://doi.org/10.1039/D3TA00904A.
- Fei, Y., Jiang, J., Zhang, L., Nie, P., Jiang, Y., Chen, Y., Zhuang, Q., and Ju, Z. (2024). Potassiophilic α-MoC anchored on 3D carbon host enables uniform potassium nucleation and super-stable potassium metal anodes. Chem. Eng. J. 490, 151527. https://doi.org/10.1016/j.cej.2024. 151527.
- 64. Chen, Y., Liu, Z., Lu, Y., Gao, X.-W., Zhou, J.-L., Wang, X.-C., Gu, Q.-F., and Luo, W.-B. (2024). Uniform potassium metal deposition under fast ion transportation kinetic: Porous carbon nanotube/metal-organic frameworks composite host. J. Power Sources 613, 234909. https://doi.org/10.1016/j.jpowsour.2024.234909.
- Liu, S., Yang, Y., Qian, Y., Chang, G., Zhao, X., Tang, Q., Hu, A., and Chen, X. (2022). MOF-Derived Potassiophilic CuO Nanoparticles on Carbon Fiber Cloth as Host for Stabilizing Potassium Metal Anode. ChemElectroChem 9, e202101561. https://doi.org/10.1002/celc.202101561.
- Li, X., Sun, J., Song, L., Jiang, X., Mo, X., Shen, J., and Zhou, X. (2024).
   Nanomesh NiO-modified carbon cloth for highly efficient self-supporting potassium metal anodes. Chem. Eng. J. 490, 151521. https://doi.org/10.1016/j.cej.2024.151521.
- 67. Lei, Y., Chen, M., Li, Y., Zhang, W., Zhao, D., and Zhu, Q. (2023). Dendrite-free potassium metal anode induced by in-situ phase transitions of MoS2. Mater. Today Phys. 35, 101141. https://doi.org/10.1016/j.mtphys.2023.101141.
- 68. Hao, J., Zhuang, Z., Cao, K., Gao, G., Wang, C., Lai, F., Lu, S., Ma, P., Dong, W., Liu, T., et al. (2022). Unraveling the electronegativity-dominated intermediate adsorption on high-entropy alloy electrocatalysts. Nat. Commun. 13, 2662. https://doi.org/10.1038/s41467-022-30379-4.
- Yang, Z., Li, X., and Gao, W. (2023). Quantitative prediction of surface energy of high-entropy-alloys based on intrinsic descriptors. Surf. Interfaces 42, 103442. https://doi.org/10.1016/j.surfin.2023.103442.
- Kristoffersen, H.H., and Rossmeisl, J. (2022). Local Order in AgAuCuPdPt High-Entropy Alloy Surfaces. J. Phys. Chem. C 126, 6782–6790. https://doi.org/10.1021/acs.jpcc.2c00478.
- Shiota, T., Ishihara, K., and Mizukami, W. (2025). Lowering the exponential wall: accelerating high-entropy alloy catalysts screening using local surface energy descriptors from neural network potentials. Digit. Discov. 4, 738–751. https://doi.org/10.1039/D4DD00303A.
- Kumar Katiyar, N., Biswas, K., Yeh, J.-W., Sharma, S., and Sekhar Ti-wary, C. (2021). A perspective on the catalysis using the high entropy alloys. Nano Energy 88, 106261. https://doi.org/10.1016/j.nanoen.2021. 106261.
- Pan, Y., Shan, X., Cai, F., Gao, H., Xu, J., and Zhou, M. (2024). Accelerating the Discovery of Oxygen Reduction Electrocatalysts: High-Throughput Screening of Element Combinations in Pt-Based High-Entropy Alloys. Angew. Chem. Int. Ed. Engl. 63, e202407116. https://doi.org/10.1002/anie.202407116.
- Feng, R., Zhang, C., Gao, M.C., Pei, Z., Zhang, F., Chen, Y., Ma, D., An, K., Poplawsky, J.D., Ouyang, L., et al. (2021). High-throughput design of high-performance lightweight high-entropy alloys. Nat. Commun. 12, 4329. https://doi.org/10.1038/s41467-021-24523-9.
- Biswal, P., Stalin, S., Kludze, A., Choudhury, S., and Archer, L.A. (2019).
   Nucleation and Early Stage Growth of Li Electrodeposits. Nano Lett. 19, 8191–8200. https://doi.org/10.1021/acs.nanolett.9b03548.
- Sun, C., Duan, Z., Wang, P., Zhang, X., Huang, M., Cao, F., Lin, W., Wang, H., Chen, Y., and Shi, X.-R. (2022). Modulation of graphene and graphdiyne by metaln (n = 1–5) adsorption and nucleation and the effect on hydrogen evolution reaction. Appl. Surf. Sci. 580, 152197. https://doi. org/10.1016/j.apsusc.2021.152197.



- Li, S., Zhu, H., Liu, Y., Han, Z., Peng, L., Li, S., Yu, C., Cheng, S., and Xie, J. (2022). Codoped porous carbon nanofibres as a potassium metal host for nonaqueous K-ion batteries. Nat. Commun. 13, 4911. https://doi.org/ 10.1038/s41467-022-32660-y.
- Feng, Y., Rao, A.M., Zhou, J., and Lu, B. (2023). Selective Potassium Deposition Enables Dendrite-Resistant Anodes for Ultrastable Potassium-Metal Batteries. Adv. Mater. 35, e2300886. https://doi.org/ 10.1002/adma.202300886.
- Yan, K., Lu, Z., Lee, H.-W., Xiong, F., Hsu, P.-C., Li, Y., Zhao, J., Chu, S., and Cui, Y. (2016). Selective deposition and stable encapsulation of lithium through heterogeneous seeded growth. Nat. Energy 1, 16010. https://doi.org/10.1038/nenergy.2016.10.
- Xie, J., Ji, Y., Ma, L., Wen, Z., Pu, J., Wang, L., Ding, S., Shen, Z., Liu, Y., Li, J., et al. (2023). Bifunctional Alloy/Solid-Electrolyte Interphase Layer for Enhanced Potassium Metal Batteries Via Prepassivation. ACS Nano 17, 1511–1521. https://doi.org/10.1021/acsnano.2c10535.
- Zhou, J., Zhao, L., Lu, Y., Gao, X., Chen, Y., Liu, Z., Gu, Q., and Luo, W. (2024). Bark-Inspired Functional-Carbon/Potassium Composite Electrode with Fast Ion Transport Channels for Dendrite-Free Potassium Metal Batteries. Adv. Funct. Mater. 34, 2403754. https://doi.org/10.1002/adfm.202403754.
- Cheng, G., Liu, S., Su, Y., Wang, X., Li, X., Shi, J., Huang, M., Shi, Z., and Wang, H. (2022). Bi@hollow carbon tube enabled high performance potassium metal batteries. J. Alloys Compd. 913, 165329. https://doi.org/ 10.1016/j.jallcom.2022.165329.
- Zhang, D.-T., Liu, M.-C., Li, M.-P., Yuan, Z.-Z., Hu, Y.-X., Chen, H., Li, C.-Y., Kong, L.-B., Zhao, K., Ren, J.-Q., et al. (2024). One-stone, two birds: Three-dimensional structure and rich-inorganic solid electrolyte interface derived from Bi nanoparticles modified Ti3C2/CNT/rGO aerogel for anode-free potassium metal batteries. Chem. Eng. J. 482, 148896. https://doi.org/10.1016/j.cej.2024.148896.
- 84. Li, H.-Y., Li, M.-P., Zhang, D.-T., Chen, H., Li, C.-Y., Shi, W.-J., Xue, H.-T., and Liu, M.-C. (2024). A "two-pronged" strategy towards dendrite-free potassium metal anodes: Potassiophilic zinc modification synergized with in-situ red phosphorus-derived protective layer. Electrochim. Acta 479, 143880. https://doi.org/10.1016/j.electacta.2024.143880.
- Yang, Q., Ding, Y., and He, G. (2020). An amalgam route to stabilize potassium metal anodes over a wide temperature range. Chem. Commun. (Camb) 56, 3512–3515. https://doi.org/10.1039/D0CC00171F.
- Han, M., Jiang, J., Lu, S., Jiang, Y., Ma, W., Liu, X., Zhao, B., and Zhang, J. (2022). Moderate Specific Surface Areas Help Three-Dimensional Frameworks Achieve Dendrite-Free Potassium-Metal Anodes. ACS Appl. Mater. Interfaces 14, 900–909. https://doi.org/10.1021/acsami. 1c19742.
- Zhang, D., Liu, M., Shi, W., Qiu, Y., Hu, Y., Yuan, Z., Xue, H., Kong, L., Zhao, K., Ren, J., et al. (2024). Dual-Gradient Engineering of Conductive and Hierarchically Potassiophilic Network for Highly Stable Potassium Metal Anode. Adv. Energy Mater. 14, 2401960. https://doi.org/10.1002/aenm.202401960.
- Zhao, X., Chen, F., Liu, J., Cheng, M., Su, H., Liu, J., and Xu, Y. (2020). Enhanced surface binding energy regulates uniform potassium deposition for stable potassium metal anodes. J. Mater. Chem. A 8, 5671–5678. https://doi.org/10.1039/C9TA14226F.
- Qiao, F., Meng, J., Wang, J., Wu, P., Xu, D., An, Q., Wang, X., and Mai, L. (2021). Building carbon cloth-based dendrite-free potassium metal anodes for potassium metal pouch cells. J. Mater. Chem. A 9, 23046–23054. https://doi.org/10.1039/D1TA06327H.
- Qi, J., Lin, C., Deng, S., Zuo, Y., Zheng, H., Jiao, X., Yan, W., and Zhang, J. (2024). Synergy of Cu-foam/Sb<sub>2</sub> Q<sub>3</sub> /rGO for stable potassium anodes of high rate and low-temperature potassium metal batteries. J. Mater. Chem. A 12, 6968–6982. https://doi.org/10.1039/D3TA06919B.
- 91. Xia, S., Xu, H., Zou, H., Shang, M., Li, L., Ouyang, B., and Zhang, W. (2024). A 3D structural NC/ZnO@carbon cloth matrix as a potassiophilic

- host for a dendrite-free potassium metal anode. Inorg. Chem. Front. 11, 5043–5053. https://doi.org/10.1039/D4QI01281J.
- Zhang, D.-T., Liu, M.-C., Li, M.-P., Chen, H., Li, C.-Y., Hu, Y.-X., Kong, L.-B., Zhang, X.-Y., Gu, B.-N., Liu, M.-J., et al. (2023). Design of a potassio-philic 3D conductive scaffold potassium anode (3D-CTZ@K) with dendrite-free and high energy-power density in potassium metal batteries. J. Mater. Chem. A 11, 20741–20751. https://doi.org/10.1039/D3TA03427F
- Sun, Z., Liu, M., Liu, B., Khan, R., Zhao, J., Huang, L., and Wu, Y. (2023). Dynamically Evolving Multifunctional Protective Layer for Highly Stable Potassium Metal Anodes. ACS Appl. Mater. Interfaces 15, 58429–58436. https://doi.org/10.1021/acsami.3c14009.
- Li, H., Zhao, C., Yin, Y., Zou, Y., Xia, Y., An, Q., Jian, Z., and Chen, W. (2020). N-Doped carbon coated bismuth nanorods with a hollow structure as an anode for superior-performance potassium-ion batteries. Nanoscale 12, 4309–4313. https://doi.org/10.1039/C9NR09867D.
- 95. Yi, Z., Qian, Y., Jiang, S., Li, Y., Lin, N., and Qian, Y. (2020). Self-wrinkled graphene as a mechanical buffer: A rational design to boost the K-ion storage performance of Sb2Se3 nanoparticles. Chem. Eng. J. 379, 122352. https://doi.org/10.1016/j.cej.2019.122352.
- Sultana, I., Ramireddy, T., Rahman, M.M., Chen, Y., and Glushenkov, A. M. (2016). Tin-based composite anodes for potassium-ion batteries. Chem. Commun. (Camb) 52, 9279–9282. https://doi.org/10.1039/C6CC03649J.
- Huang, K., Xing, Z., Wang, L., Wu, X., Zhao, W., Qi, X., Wang, H., and Ju, Z. (2018). Direct synthesis of 3D hierarchically porous carbon/Sn composites via in situ generated NaCl crystals as templates for potassiumion batteries anode. J. Mater. Chem. A 6, 434–442. https://doi.org/10.1039/C7TA08171E.
- Hu, J., Wang, H., Wang, S., Lei, Y., Qin, L., Li, X., Zhai, D., Li, B., and Kang, F. (2021). Electrochemical deposition mechanism of sodium and potassium. Energy Storage Mater. 36, 91–98. https://doi.org/10.1016/j. ensm 2020 12 017
- Yang, H., He, F., Li, M., Huang, F., Chen, Z., Shi, P., Liu, F., Jiang, Y., He, L., Gu, M., et al. (2021). Design Principles of Sodium/Potassium Protection Layer for High-Power High-Energy Sodium/Potassium-Metal Batteries in Carbonate Electrolytes: a Case Study of Na<sub>2</sub> Te/K<sub>2</sub> Te. Adv. Mater. 33, e2106353. https://doi.org/10.1002/adma.202106353.
- Wu, H., Jia, H., Wang, C., Zhang, J.-G., and Xu, W. (2021). Recent Progress in Understanding Solid Electrolyte Interphase on Lithium Metal Anodes. Adv. Energy Mater. 11, 2003092. https://doi.org/10.1002/aenm. 202003092.
- Yamaki, J., Tobishima, S., Hayashi, K., Saito, K., Nemoto, Y., and Arakawa, M. (1998). A consideration of the morphology of electrochemically deposited lithium in an organic electrolyte. Journal of Power Sources 74, 219–227. https://doi.org/10.1016/S0378-7753(98)00067-6.
- 102. Li, Y., Li, Y., Pei, A., Yan, K., Sun, Y., Wu, C.-L., Joubert, L.-M., Chin, R., Koh, A.L., Yu, Y., et al. (2017). Atomic structure of sensitive battery materials and interfaces revealed by cryo–electron microscopy. Science 358, 506–510. https://doi.org/10.1126/science.aam6014.
- 103. Li, Y., Huang, W., Li, Y., Pei, A., Boyle, D.T., and Cui, Y. (2018). Correlating Structure and Function of Battery Interphases at Atomic Resolution Using Cryoelectron Microscopy. Joule 2, 2167–2177. https://doi.org/10.1016/j.joule.2018.08.004.
- 104. Gao, Y., Hou, Z., Zhou, R., Wang, D., Guo, X., Zhu, Y., and Zhang, B. (2022). Critical Roles of Mechanical Properties of Solid Electrolyte Interphase for Potassium Metal Anodes. Adv. Funct. Mater. 32, 2112399. https://doi.org/10.1002/adfm.202112399.
- 105. Gao, Y., Du, X., Hou, Z., Shen, X., Mai, Y.-W., Tarascon, J.-M., and Zhang, B. (2021). Unraveling the mechanical origin of stable solid electrolyte interphase. Joule 5, 1860–1872. https://doi.org/10.1016/j.joule. 2021.05.015.





- 106. Gu, Y., Wang, W.-W., Li, Y.-J., Wu, Q.-H., Tang, S., Yan, J.-W., Zheng, M.-S., Wu, D.-Y., Fan, C.-H., Hu, W.-Q., et al. (2018). Designable ultra-smooth ultra-thin solid-electrolyte interphases of three alkali metal anodes. Nat. Commun. 9, 1339. https://doi.org/10.1038/s41467-018-03466-8.
- 107. Yim, C.-H., Tam, J., Soboleski, H., and Abu-Lebdeh, Y. (2017). On the Correlation between Free Volume, Phase Diagram and Ionic Conductivity of Aqueous and Non-Aqueous Lithium Battery Electrolyte Solutions over a Wide Concentration Range. J. Electrochem. Soc. 164, A1002–A1011. https://doi.org/10.1149/2.1601704jes.
- 108. Park, S., Chaudhary, R., Han, S.A., Qutaish, H., Moon, J., Park, M.-S., and Kim, J.H. (2023). Ionic conductivity and mechanical properties of the solid electrolyte interphase in lithium metal batteries. Energy Mater. 3, N/A-N/A. https://doi.org/10.20517/energymater.2022.65.
- Nojabaee, M., Küster, K., Starke, U., Popovic, J., and Maier, J. (2020).
   Solid Electrolyte Interphase Evolution on Lithium Metal in Contact with Glyme-Based Electrolytes. Small 16, e2000756. https://doi.org/10. 1002/smll.202000756.
- 110. Deng, W., Yu, Z., Yang, H., Chen, Z., Zheng, J., He, Z., Shao, Y., Jiao, S., Tao, X., Shen, Y., et al. (2024). Balancing Potassiophilicity and Catalytic Activity of Artificial Interface Layer for Dendrite-Free Sodium/Potassium Metal Batteries. Adv. Mater. 36, e2412446. https://doi.org/10.1002/adma.202412446.
- 111. Wang, H., Hu, J., Dong, J., Lau, K.C., Qin, L., Lei, Y., Li, B., Zhai, D., Wu, Y., and Kang, F. (2019). Artificial Solid-Electrolyte Interphase Enabled High-Capacity and Stable Cycling Potassium Metal Batteries. Adv. Energy Mater. 9, 1902697. https://doi.org/10.1002/aenm.201902697.
- 112. Park, J., Jeong, Y., Alfaruqi, M.H., Liu, Y., Xu, X., Xiong, S., Jung, M.-G., Jung, H.-G., Kim, J., Hwang, J.-Y., et al. (2022). Stable Solid Electrolyte Interphase for Long-Life Potassium Metal Batteries. ACS Energy Lett. 7, 401–409. https://doi.org/10.1021/acsenergylett.1c02354.
- 113. Ells, A.W., May, R., and Marbella, L.E. (2021). Potassium Fluoride and Carbonate Lead to Cell Failure in Potassium-Ion Batteries. ACS Appl. Mater. Interfaces 13, 53841–53849. https://doi.org/10.1021/acsami. 1c15174.
- 114. Baek, S., Jie, S., and Lee, B. (2023). Effects of fluoroethylene carbonate additive on potassium metal anode. J. Mech. Sci. Technol. 37, 3657– 3665. https://doi.org/10.1007/s12206-023-0630-3.
- 115. Jiang, J., Liu, Y., Liao, Y., Li, W., Xu, Y., Liu, X., Jiang, Y., Zhang, J., and Zhao, B. (2023). Construction of Synchronous-Deposition K Metal Anodes Via Modulation of Ion/Electron Transport Kinetics for High Rate and Low-Temperature K Metal Batteries. Small 19, e2300854. https:// doi.org/10.1002/smll.202300854.
- 116. Shi, P., Zhang, S., Lu, G., Wang, L., Jiang, Y., Liu, F., Yao, Y., Yang, H., Ma, M., Ye, S., et al. (2021). Red Phosphorous-Derived Protective Layers with High Ionic Conductivity and Mechanical Strength on Dendrite-Free Sodium and Potassium Metal Anodes. Adv. Energy Mater. 11, 2003381. https://doi.org/10.1002/aenm.202003381.
- 117. Thaman, H.L., Li, M., Rose, J.A., Narasimhan, S., Xu, X., Yeh, C.-N., Jin, N., Akbashev, A., Davidoff, I., Bazant, M.Z., et al. (2025). Two-Stage Growth of Solid Electrolyte Interphase on Copper: Imaging and Quantification by Operando Atomic Force Microscopy. ACS Nano 19, 11949–11960. https://doi.org/10.1021/acsnano.4c16418.
- 118. Capone, F.G., Sottmann, J., Meunier, V., Pérez Ramírez, L., Grimaud, A., ladecola, A., Scardamaglia, M., Rueff, J.-P., and Dedryvère, R. (2024). Operando observation of the dynamic SEI formation on a carbonaceous electrode by near-ambient pressure XPS. Energy Environ. Sci. 17, 1509–1519. https://doi.org/10.1039/D3EE03228K.
- Krumov, M.R., Lang, S., Johnson, L., and Abruña, H.D. (2023). Operando Investigation of Solid Electrolyte Interphase Formation, Dynamic Evolution, and Degradation During Lithium Plating/Stripping. ACS Appl. Mater. Interfaces 15, 47692–47703. https://doi.org/10.1021/acsami.3c08485.
- Dachraoui, W., Pauer, R., Battaglia, C., and Erni, R. (2023). Operando Electrochemical Liquid Cell Scanning Transmission Electron Microscopy

- Investigation of the Growth and Evolution of the Mosaic Solid Electrolyte Interphase for Lithium-Ion Batteries. ACS Nano *17*, 20434–20444. https://doi.org/10.1021/acsnano.3c06879.
- 121. Teng, W., Wu, J., Liang, Q., Deng, J., Xu, Y., Liu, Q., Wang, B., Ma, T., Nan, D., Liu, J., et al. (2023). Designing Advanced Liquid Electrolytes for Alkali Metal Batteries: Principles, Progress, and Perspectives. Energy & Environ. Materials 6, e12355. https://doi.org/10.1002/eem2.12355.
- 122. Jie, Y., Wang, S., Weng, S., Liu, Y., Yang, M., Tang, C., Li, X., Zhang, Z., Zhang, Y., Chen, Y., et al. (2024). Towards long-life 500 Wh kg-1 lithium metal pouch cells via compact ion-pair aggregate electrolytes. Nat. Energy 9, 987–998. https://doi.org/10.1038/s41560-024-01565-z.
- 123. Kim, S.C., Wang, J., Xu, R., Zhang, P., Chen, Y., Huang, Z., Yang, Y., Yu, Z., Oyakhire, S.T., Zhang, W., et al. (2023). High-entropy electrolytes for practical lithium metal batteries. Nat. Energy 8, 814–826. https://doi.org/10.1038/s41560-023-01280-1.
- 124. Jang, J., Wang, C., Kang, G., Han, C., Han, J., Shin, J.-S., Ko, S., Kim, G., Baek, J., Kim, H.-T., et al. (2025). Miniature Li+ solvation by symmetric molecular design for practical and safe Li-metal batteries. Nat. Energy 10, 502–512. https://doi.org/10.1038/s41560-025-01733-9.
- 125. Ma, X., Zhang, D., Fu, H., Rao, A.M., Zhou, J., Fan, L., and Lu, B. (2025). Energy band-engineered solid electrolyte interphase for stable potassium-ion batteries. Joule 9, 101952. https://doi.org/10.1016/j.joule. 2025.101952.
- Singla, A., Naik, K.G., Vishnugopi, B.S., and Mukherjee, P.P. (2024). Heterogeneous Solid Electrolyte Interphase Interactions Dictate Interface Instability in Sodium Metal Electrodes. Adv. Sci. (Weinh) 11, e2404887. https://doi.org/10.1002/advs.202404887.
- 127. Weeks, J.A., Burrow, J.N., Diao, J., Paul-Orecchio, A.G., Srinivasan, H. S., Vaidyula, R.R., Dolocan, A., Henkelman, G., and Mullins, C.B. (2024). In Situ Engineering of Inorganic-Rich Solid Electrolyte Interphases via Anion Choice Enables Stable, Lithium Anodes. Adv. Mater. 36, e2305645. https://doi.org/10.1002/adma.202305645.
- 128. Xu, Y., Dong, K., Jie, Y., Adelhelm, P., Chen, Y., Xu, L., Yu, P., Kim, J., Kochovski, Z., Yu, Z., et al. (2022). Promoting Mechanistic Understanding of Lithium Deposition and Solid-Electrolyte Interphase (SEI) Formation Using Advanced Characterization and Simulation Methods: Recent Progress, Limitations, and Future Perspectives. Adv. Energy Mater. 12, 2200398. https://doi.org/10.1002/aenm.202200398.
- 129. Sheng, O., Zheng, J., Ju, Z., Jin, C., Wang, Y., Chen, M., Nai, J., Liu, T., Zhang, W., Liu, Y., et al. (2020). In Situ Construction of a LiF-Enriched Interface for Stable All-Solid-State Batteries and its Origin Revealed by Cryo-TEM. Adv. Mater. 32, e2000223. https://doi.org/10.1002/adma.202000223
- 130. Ji, Y., Qiu, J., Zhao, W., Liu, T., Dong, Z., Yang, K., Zheng, G., Qian, G., Yang, M., Chen, Q., et al. (2023). In situ probing the origin of interfacial instability of Na metal anode. Chem 9, 2943–2955. https://doi.org/10.1016/j.chempr.2023.06.002.
- Bak, S.-M., Shadike, Z., Lin, R., Yu, X., and Yang, X.-Q. (2018). In situ/operando synchrotron-based X-ray techniques for lithium-ion battery research. NPG Asia Mater. 10, 563–580. https://doi.org/10.1038/s41427-018-0056-z.
- Sukumaran, S., Fearn, S., and Skinner, S.J. (2025). In situ TOF-SIMS investigation of the dynamic metallic anode|solid electrolyte interface in solid-state sodium-ion batteries. Physiol. Sci. 6. https://doi.org/10.1016/j.xcrp.2025.102447.
- 133. Bhattacharyya, R., Key, B., Chen, H., Best, A.S., Hollenkamp, A.F., and Grey, C.P. (2010). In situ NMR observation of the formation of metallic lithium microstructures in lithium batteries. Nat. Mater. 9, 504–510. https://doi.org/10.1038/nmat2764.
- 134. Gu, Y., You, E.-M., Lin, J.-D., Wang, J.-H., Luo, S.-H., Zhou, R.-Y., Zhang, C.-J., Yao, J.-L., Li, H.-Y., Li, G., et al. (2023). Resolving nano-structure and chemistry of solid-electrolyte interphase on lithium anodes





- by depth-sensitive plasmon-enhanced Raman spectroscopy. Nat. Commun. 14, 3536. https://doi.org/10.1038/s41467-023-39192-z.
- 135. Zhang, W., Weng, M., Zhang, M., Ye, Y., Chen, Z., Li, S., Li, S., Pan, F., and Wang, L. (2023). Revealing Morphology Evolution of Lithium Dendrites by Large-Scale Simulation Based on Machine Learning Force Field. Adv. Energy Mater. 13, 2202892. https://doi.org/10.1002/aenm. 202202892.
- Choi, G., Kim, Y., Choi, J., and Kim, D. (2022). Thermodynamic Factor for Facilitating Homogeneous Dendrite Growth in Alkali Metal Batteries. Adv. Energy Mater. 12, 2201428. https://doi.org/10.1002/aenm.202201428.
- Gao, L., and Guo, Z. (2020). Phase-field simulation of Li dendrites with multiple parameters influence. Comput. Mater. Sci. 183, 109919. https://doi.org/10.1016/j.commatsci.2020.109919.
- 138. Wang, Q., Zhang, G., Li, Y., Hong, Z., Wang, D., and Shi, S. (2020). Application of phase-field method in rechargeable batteries. npj Comput. Mater. 6, 1–8. https://doi.org/10.1038/s41524-020-00445-w.
- 139. Tan, X., Chen, M., Zhang, J., Li, S., Zhang, H., Yang, L., Sun, T., Qian, X., and Feng, G. (2024). Decoding Electrochemical Processes of Lithium-Ion Batteries by Classical Molecular Dynamics Simulations. Adv. Energy Mater. 14, 2400564. https://doi.org/10.1002/aenm.202400564.